ISTANBUL TECHNICAL UNIVERSITY ★ GRADUATE SCHOOL OF SCIENCE ENGINEERING AND TECHNOLOGY

MODELLING AND DETERMINATION OF LOOSENING MECHANISM OF BOLTED JOINTS IN WASHING MACHINE

M.Sc. THESIS

Onur KONUK

Department of Mechanical Engineering

Solid Mechanics Program

JULY 2020

ISTANBUL TECHNICAL UNIVERSITY ★ GRADUATE SCHOOL OF SCIENCE ENGINEERING AND TECHNOLOGY

MODELLING AND DETERMINATION OF LOOSENING MECHANISM OF BOLTED JOINTS IN WASHING MACHINE

M.Sc. THESIS

Onur KONUK
(503171510)

Department of Mechanical Engineering

Solid Mechanics Program

Thesis Advisor: Prof. Dr. Ata MUĞAN

JULY 2020

İSTANBUL TEKNİK ÜNİVERSİTESİ ★ FEN BİLİMLERİ ENSTİTÜSÜ

ÇAMAŞIR MAKİNASINDA BULUNAN CİVATA BAĞLANTILARININ MODELLENEREK ÇÖZÜLME MEKANİZMASININ BELİRLENMESİ

YÜKSEK LİSANS TEZİ

Onur KONUK
(503171510)

Makina Mühendisliği Anabilim Dalı

Katı Cisimlerin Mekaniği Programı

Tez Danışmanı: Prof. Dr. Ata MUĞAN

TEMMUZ 2020

Onur KONUK, a M.Sc. student of ITU Graduate School of Science Engineering And Technology student ID 503171510, successfully defended the thesis entitled "MODELLING AND DETERMINATION OF LOOSENING MECHANISM OF BOLTED JOINTS IN WASHING MACHINE ", which he prepared after fulfilling the requirements specified in the associated legislations, before the jury whose signatures are below.

Thesis Advisor :	**Prof. Dr. Ata MUĞAN** Istanbul Technical University	.....
Jury Members :	**Assoc. Prof. Zeki Yağız BAYRAKTAROĞLU** Istanbul Technical University	.....
	Assoc. Prof. Cüneyt YILMAZ Yıldız Technical University	.....

Date of Submission :15 June 2020
Date of Defense :21 July 2020

To my family,

FOREWORD

I would like to utter deference and thankfulness to my advisor Prof. Dr. Ata MUĞAN who encouraged and enlightened me throughout the whole study, despite many challenging conditions and adversity.

I would like to express my gratefulness to ARCELIK A.S Washing Machine Plant Director Atilla UZ and WMP Research & Development Group Manager Ümit GÜLBAY for the support of my research. I would like to express my appreciation WMP R&D Structural Design Manager Burçin SOMER and WMP Quality Assurance Manager Seyhun BAKIRHAN for their guidance.

I would like to express my sincere appreciation WMP R&D Structural Design Team Leader Yunus Emre AYDOĞDU for moral and dedicated technical support with his valuable experiences during my master thesis.

Also, I would like to thank all of my friends for their unique motivation.

Finally, I would like to thank and dedicate my master thesis to my beloved fiancée and family who always stand by me with their infinite support.

July 2020

Onur KONUK
(Mechanical Engineer)

TABLE OF CONTENTS

Page

ABBREVIATIONS

FFT	**:** Fast Fourier Transform
FRF	**:** Frequency Response Function
CAD	**:** Computer-Aided Drawing
CAE	**:** Computer-Aided Engineering
FEA	**:** Finite Element Analysis
FEM	**:** Finite Element Method
RPM	**:** Revolutions Per Minute
DOF	**:** Degree of Freedom
Hz	**:** Hertz
mm	**:** Millimeters
m	**:** Meters
m/s	**:** Meters per second
kg	**:** Kilograms
N	**:** Newtons
kg-f	**:** Kilogram Force
kN	**:** Kilo Newtons
N.cm	**:** Newton centimeter

LIST OF TABLES

Page

LIST OF FIGURES

Page

MODELLING AND DETERMINATION OF LOOSENING MECHANISM OF BOLTED JOINTS IN WASHING MACHINE

SUMMARY

In constructional engineering, bolted joints are the most used machine components in assembly of different parts. Since it is widely used, there are several failure modes of bolted joints. In order to prevent engineering failures, there are common precautions such as special lock washers, nylon or metal inserts which prevail torque from loosening, double nuts, adhesives etc. Most of these methods are irreversible and not feasible for mass production such as household products. Thus, modelling and analyzing of bolted joints have become very significant in past century. It is not possible to check quality of every single threaded fastener in a washing machine.

Major aim is to suggest a theoretical and experimental static and dynamic model for bolted joints in washing machine to check connections is cope of loosening without decoupling the assembly. There have been various research and studies for modelling of bolted joints. Initially, static modelling is quite basic for primary construction designs. This model solely covers the initial elongations and safety procedures. In static model, bolted joints are considered as linear spring elements but this method does not meet the requirements of real circumstances. Although, there are many different bolted joints which are affected by their variable environmental conditions, such as dynamic loadings. Both static and dynamic behavior of bolted joints have been examined. It is very important to model threaded regions within both static and dynamic. Most of the studies does not provide a theoretical model that includes how much preload actually have been transmitted into clamping threads itself. In some of the studies, bolted joints are modeled with spring and damping element. Damping element is here to represent energy dissipation due to contact of threads. Moreover, these models do not fulfill because, it is still neglecting non – linear effects. Modelling of friction between mating threads is very burdensome yet it is necessary to govern loosening model of threaded fasteners. To acquire certain parameters, empirical expressions are proposed regarding different experimental data. There are a variety of different bolted joints experiments. Modal testing of well-structured lap joints is the common test rig in order to determine characteristics of the connection.

Although, it is widely common that testing on generalized test components, main goal is to create a set of procedure for testing loosening of washing machine threaded connections and bolted joints. Determination parameters and quality of coupled structures in mass production such as laundry is quite vital for the end user of the products and serviceability. In mass productions, parts are assembled with multiple bolted joints or screws. There has not been any research which includes detection of defected joint in complex structures such as washing machine.

In this study, both theoretical and experimental data have been compared for verification. Theoretical calculations have been made in MATLAB. For the experiment, particular test rigs have been reviewed and all of the test rigs represents general conditions which are not fully satisfying washing machine connections.

Experimental data have been taken from current individual washing machine and test have been conducted in Arcelik Cayirova, Washing Machine Plant, R&D.

ÇAMAŞIR MAKİNASINDA BULUNAN CİVATA BAĞLANTILARININ MODELLENEREK ÇÖZÜLME MEKANİZMASININ BELİRLENMESİ

ÖZET

Cıvatalı bağlantılar konstrüksiyon mühendisliğinde oldukça yaygın olarak kullanılan makine elemanlarıdır. Geniş endüstriyel alanlarda, yaygın kullanılması doğrultusunda, cıvatalı bağlantıların birden çok hata mekanizması gözlenmiştir. Bu mekanizmalardan en önemlisi bağlantının ön gerilme düşüşüne bağlı olarak tork kaybıdır. Cıvatalı bağlantılarda tork düşüşünü engellemek için, kilitli rondela, plastik veya metal insert, çift somun, yapıştırıcı özelliği bulunan adhezivler vb. gibi çözümler uygulanmaktadır. Bu tip önlemler, beyaz eşya sektörü gibi seri üretim hattına sahip işletmeler için değerlendirildiğinde, maliyetli olmakla birlikte verimsizlik yaratmaktadır. Beyaz eşya üreticileri gibi yüksek hacimli üretimin bulunduğu durumlarda montajlanan her vidanın yeterliliğinin mevcut metotlarla ölçümü zaman kaybına yol açmaktadır.

Ana amaç, bağlantıları kontrol etmek kapsamında çamaşır makinesindeki cıvatalı bağlantılar için teorik ve deneysel, statik ve dinamik bir model geliştirilerek montajlı parçaları sökmeden gevşemenin başlangıcı tespitini yapabilmektir.

Cıvatalı bağlantıların modellenmesi için çeşitli araştırmalar ve çalışmalar yapılmıştır. Başlangıçta, statik modelleme birincil inşaat tasarımları için oldukça basittir. Bu model sadece ilk uzamaları ve güvenlik prosedürlerini kapsar. Statik modelde, cıvatalı bağlantılar doğrusal yay elemanları olarak kabul edilir, ancak bu yöntem gerçek koşulların gereksinimlerini karşılamaz. Bununla birlikte, dinamik yüklemeler gibi değişken çevresel koşullarından etkilenen birçok farklı cıvatalı bağlantı vardır. Cıvatalı bağlantıların hem statik hem de dinamik davranışı incelenmiştir. Dişli bölgelerin hem statik hem de dinamik olarak modellenmesi çok önemlidir. Çalışmaların çoğu, gerçekte ne kadar ön yükün kenetleme dişlerinin kendisine aktarıldığını içeren teorik bir model sağlamamaktadır.

Bazı çalışmalarda cıvatalı bağlantılar yay ve sönümleme elemanı ile modellenmiştir. Sönümleme elemanı, dişlerin teması nedeniyle enerji yayılımını temsil etmek için buradadır. Dahası, bu modeller tatmin edici değildir, çünkü hala doğrusal olmayan etkileri ihmal etmektedir. Cıvata – somun dişleri arasındaki sürtünmenin non lineer modellenmesi karmaşık olmakla birlikte, bağlantıların gevşeme mekanizmasını tanımlanması için üstünde durulması gereken bir husustur. Cıvata modellenmesiyle ilgili öncü çalışmalarda belirli parametreleri elde etmek için farklı deneysel verilerle ampirik ifadeler önerilerek yaklaşımlar sunulmuş, bu çalışmalar tez içerisinde incelenmiştir. Bu çalışmalardan bazıları sadece statik olup genel sürtünme yaklaşımıyla yorumlanmıştır. Bir diğer modelleme yöntemi ise bağlantıyı kütle, katı yay, viskoz sönüm ve statik sürtünme ile modellenmiştir. Bu çalışmada üzerinde durulan metot ise Basitleştirilmiş Iwan Modeli ve Pim Etkisi modeli olup cıvataların çalışmasına bağlı olarak enerji üzerinden kayar yaylı elemanlarla modellenmesini içermektedir. Bu modellemede en önemli parametre kayar yaylı elemanların yoğunluk fonksiyonudur ve bu fonksiyon basitleştirilmemiş durumlarda her yükleme ve her tasarım için farklı şekilde oluşmaktadır. Basitleştirilmiş modelde bu yüklemelerin

oluşturduğu histerik modeller bir önceki adımda oluşan histerik modelin genişletişmiş versiyonu, bir çarpanı, olarak kabul edilmiştir. Yapılan bu basitleştirmeyle hesaplama yükü oldukça azalmıştır.

Günümüzde cıvatalı bağlantıların irdelenmesinde modal test yöntemi, güvenilir ve sistematik yöntemlerden biridir. Tez içerisinde incelenen çalışmalarda modal test deney yöntemli çoklukla vatkalı (bindirmeli) cıvatalı bağlantılarda uygulanmıştır. Modal test, göbek tipli (bosslu) cıvatalı bağlantılarda ilk olarak bu tez kapsamında deney yapılmıştır.

Genel test bileşenleri üzerinde test yapılması yaygın olsa da ana amaç, çamaşır makinesi dişli bağlantılarının ve cıvatalı bağlantıların gevşemesini test etmek için bir dizi prosedür oluşturmaktır. Çamaşır gibi seri üretimde birleştirilmiş yapıların belirleme parametreleri ve kalitesi, ürünlerin son kullanıcısı ve servis kolaylığı için son derece önemlidir. Seri üretimlerde, parçalar çoklu cıvatalı bağlantı veya vidalarla monte edilir. Çamaşır makinesi gibi karmaşık yapılarda kusurlu bağlantının tespitini içeren herhangi bir araştırma bugüne dek yapılmamıştır.

Bu çalışmada çamaşır makinelerinde bulunan bağlantıların genel olarak modellenebilmesi ve kendi kendine çözülme kusuru görülmeden tespit edilmesini sağlayacak yöntem geliştirilmesi amaçlanmıştır. Bu yöntemin geliştirilmesi safhasında cıvataların bağlı bulunduğu parçalara ve birbirilerine göre ilişkileri irdelenmiştir. Farklı sıkma torklarıyla ve deneyle incelenen parametreler, kuvvet iletim karakteristiği, mod frekansları ve ani faz değişimleridir. Zamana bağlı titreşimli uyarılma için ise sıka torkuyla oluşan ön gerilmenin değişimi gözlenmiştir. Yapılan deneyler sonucunda çamaşır makinalarının denge ağırlığı vidalarında cıvata davranışlarının değiştiği limit torklar ortaya konmuş olup ani faz değişimleriyle desteklenmiştir. Ani faz değişiklikleri cıvatanın mikro ve makro kayma davranışlarının modellenmesinde önemli bir parametre olup farklı tork değerleriyle bu davranışların yorumu ortaya konmuştur. Ön gerilme değeri düşümlerinin gözlendiği deneylerde uyarım frekansları ve tekrarlarının düşüş karakteristiğine non lineer olarak etkilediği deneyler ile saptanmıştır. Ayrıca ön gerilmede bağlantının polimer malzeme içermesinden dolayı viskoelastik davranışın etkisi gözlenmiştir.

Deney sonuçlarının teoride verilen sonuçlarla karşılaştırması sonucunda bağlantı tasarımı ve malzemeleri nedenli farklılıklar ortaya konmuştur. Teoride verilen karakteristik eğrilerine karşılık deney sonucunda non lineer etkilerin ön planda olduğu eğriler elde edilmiştir. Bu eğrilerin karşılaştırılması sonucunda hem mikro kayma ve makro kayma hem de viskoelastik etkilerden dolayı farklılıkların kaynaklandığı tespit edilmiştir.

Deney sonuçları ışığında çamaşır makinesi seri üretim hatlarında vida tork sistemlerinde bir kontrol algoritmasına temel olabilecek limit değerlerin tespiti yapılmıştır. Bu çalışma çamaşır makinesi seri üretim hatlarında otomasyon ile uygulanması montajlanan vidanın kalitesine dair parametreler çıkarılmasına olanak tanıyacaktır. Bu çalışma dengelem ağırlıklarının vidalarında uygulanmasına rağmen farklı tasarımda vidalarda deneylerle ile desteklenerek ilgili vidaların modellenmesine katkı sağlamaktadır. Bu çalışmada uygulanan deneyler farklı kapasite ve devirdeki çamaşır makinelerinin bağlantıları için uygulanarak parametre elde etmek mümkün olacaktır.

Teorik kıyaslamada baz alınan cıvata modellemesinin yanı sıra kamyon makas yaylarının modellenmesiyle analoji yapılarak cıvataların histerik davranışlarından

parametre elde edilmesi incelenmiştir. Buna yönelik cıvata üzerinden histerik grafik elde edilmesine yönelik program üzerinde çalışılmıştır.

Viskoelastik incelemeye yönelik önceki adım zamanına bağlı uygulana gerilmelerin ve birim uzamaların ilgili parçanın sonraki davranışı etkilediği deneyler sırasında gözlemlenmiştir. Bu yaklaşım göz önünde bulundurularak kesirli diferansiyel yaklaşımı irdelenmiştir. Bu yaklaşım mevcut lineer viskoelastik incelemesinin hesaplama yükünü azaltmaktadır.

Yüksek hacimli üretim platformlarında bağlantı kalitelerini artıracak ve tahribatsız sökme işlemi gerçekleşmeden cıvata hakkında bilgi sahibi olmayı sağlayacak metodun yanı sıra çözülmeye başlamadan cıvatanın hasara uğrayacağını tahmin edebilecek bir modelleme amaçlanmıştır. Bu modelleme gerçekleştirilirken modal test tekniğinden yararlanılmıştır. Modal test metodu tüm dünya genelinde bir yapının farklı frekans uyarımları altında davranışını öngörümünü sağlayan en önemli metotlardan biridir. Dönen cisimlerin dinamik davranışlarının mod frekans tayinlerinde yaygın olarak kullanılan metotlar arasındandır.

Çamaşır makinesi üzerinde bağlantıların çözülmesi özellikle müşteri için ağır tahribatlı ve can kaybına yol açabilecek hatalara neden olabilmektedir. Dolayısıyla montajlanma torklarının yanı sıra montajlanan vidanın akuple olması sırasında ürettiği parametrelerin irdelenmesi önem arz etmektedir. Bu parametrelerin ürün daha hattan ayrılmadan elde edilmesi tahribatlı hatanın müşteride çıkma olasılığının oldukça düşürecektir. Endüstride bağlantıların kontrolü için genellikle bağlantılar sökülmekte ve mevcut bağlantı durumu rahatsız edilerek incelenmektedir. Bağlantı sökümü gerçekleşmesinden sonra ilgili parametreler tamamen değişmekte olup akuple olduğu fazdaki özellikler yansıtmamaktadır.

Bu çalışmada cıvataya ait oluşturulan parametreler CAE ortamında yapılacak simülasyonları girdi olabilecek parametreler oluşturmaktadır. CAE simülasyonlarında yapılan kontakt modellerine non lineer cıvata modelinin tanıtılması kritik gerilme ve birim şekil değiştirme karakteristiğinin hesaplanması doğrultusunda yarar sağlayacaktır. Özellikle literatür genelinde bindirmeli bağlantılardan ziyade boss yapılı bağlantıların deneysel olarak irdelenmesi bu tasarımlarda yapılacak hesapların irdelenmesinde katkı yapacaktır.

Bu çalışmada hem teorik hem de deneysel veriler doğrulama için karşılaştırılmıştır. Teorik hesaplamalar MATLAB'da yapılmıştır. Yapılan deney ve ölçümler sonucunda çamaşır makinası bağlantılarında kullanılacak şekilde genel bir modelleme geliştirilmeye çalışılmıştır. Mevcut bireysel çamaşır makinesinden deneysel veriler alınmış ve Arçelik Çayırova, Çamaşır Makinesi İşletmesi, Ar-Ge'de gerçekleştirilmiştir.

1. INTRODUCTION

The early usage of bolted joints and threaded screws antedate to ancient times. Mechanical joints, mostly rivets and screws, had been used in fixing varied sized structures to the ground. One of the tools having threads was the clamp which used screws for pitching to hold a structure of any size for processing purposes. As all other engineering tools, bolted joints' usage has had increased after the industrial revolution starting in the 18^{th} century. With the development of steam powered engines, bolted joints were the vital machine element to be used in assembling the components together. Bolted joints grant an ease in serviceability such as in trains and railways. With the First World War and Second World War, demand for bolted joints has significantly increased due to perpetuate war machine production. [11]

1.1 Loosening of Mechanical Joints

Different types of mechanical joint failures have been occurred and observed in practice. One of the most observed failure types was self–loosening of fasteners under vibrations. Catastrophic results of such failures have leaded engineers to solve the loosening problem with a haste. Thus, adequate solutions have been suggested such as lock wires and lock washers [10].

Currently, most of the mass producers are using various types of screws and bolted joints. One of these industries is household appliances and washing machines. Since washing machine is experiencing different load types and vibrations, joint strength and improvements in mechanisms to prevent bolt loosening have significant consequences.

1.2 Literature Review

Joint loosening models can be divided into static and dynamic modeling. Firstly, static models of bolted joints which provide initial constructional requirements of assembled structure is going to be reviewed. Secondly, dynamic modeling that can be separated into linear and nonlinear modeling will be explained. Linear dynamic modeling of bolted joints that is based on governing equations of loosening motion is mostly expressed with linear spring and linear dashpot-damping elements will be described. Finally, nonlinear dynamic modeling which is the basis of joint model in this study and includes a friction model for the bolted joint will be stated.

1.2.1 Static models

Most known joint models are structured based on the Coulomb's friction. One can assume that bolt nut and threads represent a slider on the platform, which can be seen in Figure 1.1. In order to maintain a constant preload, a critical torque value is determined. The preload depends on the thread diameter, bolt head diameter, thread angle, Coulomb's friction coefficient angle between the nut and thread, friction coefficient under the bolt head and applied torque value [8]. Following, the applied torque T can be expressed as follows

$$T = F_V\left(\frac{d_2}{2}\tan(-\varphi+\rho)+\frac{D_H}{2}\mu_H\right) \tag{1.1}$$

where F_v is the axial preload, d_2 is the pitch diameter of thread, D_H friction diameter of a bolt head or nut ρ coefficient angle which is calculated with $\rho = \text{atan}\mu$, μ is friction coefficient in threads, φ is the slope or helix angle, μ_H coefficient friction in threads, under head or nut. After the tightening process, axial preload will emerge via the friction between the bolt head and bolt nut. If any separating working load exists, it will overcome the existing friction force and joint loosening process will begin.

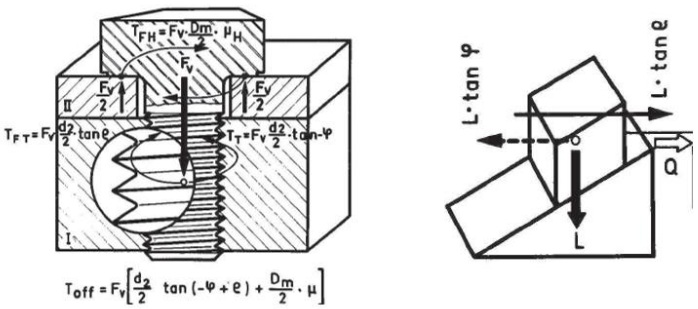

Figure 1.1 : Simplified model of threaded fasteners [8].

Among many other approximations to bolted joints, Chen et al. (2004) proposed that threaded part of a bolt is modeled by three distributed centered masses and three springs with equivalent stiffness, that is closely correlated with experimental measurements. Similarly, the nut is represented by three centered masses and three equivalent springs which can be seen in Figure 1.2. The Hooke's law is going to be applied to the threaded region of both the bolt and nut [7]. The static axial preload P_{static} in the bolt can be expressed as a linear spring as follows

$$P_{static} = K_{static} * U_{static} \tag{1.2}$$

where K_{static} is the joint stiffness and U_{static} is the static elongation of the bolt under the preload. Since contact area includes both the bolt thread and nut thread, intersection stiffness is determined with the moment–area method via an axial force moment on the threads, e.g., see Figure 1.11).

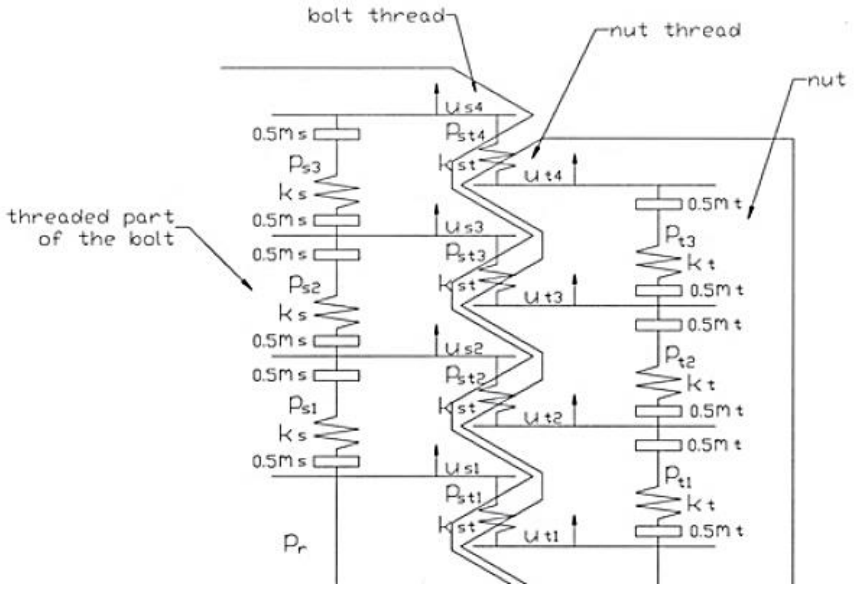

Figure 1.2 : Three masses and three springs model of the bolted joint [7].

1.2.2 Dynamic models

Dynamic modeling has become mandatory to examine self-loosening of bolted joints under vibrations since threaded fasteners are exposed to varying forces having different frequencies. Loosening of preloaded joints initially studied and published by Goodier and Sweeney in 1945. Goodier and Sweeney had conducted experiments and examined the axial load change in the loosening mechanism [6].

Gerhard H. Junker has proposed a test rig and suggested that transversely loads in bolted joints are more effective in loosening under vibrational conditions. Relative movements between flanges are being simulated with Junker's test.[8]

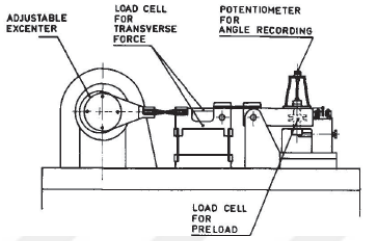

Figure 1.3 : Gerard H. Junker Test Machine Design [8].

Junker also suggested a methodology to investigate the seperating self loosening problem with other joint failure types such as fatigue failure. Loosening failure and fatigue failure show the same symptoms, nevertheless, their developing mechanisms are different. Junker's test machine can be seen in Figure 1.3 and the joint failure methodology of Junker is also presented in Figure 1.4.

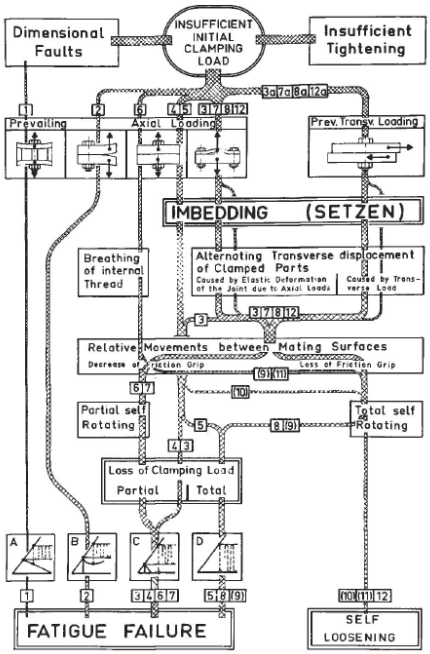

Figure 1.4 : Failure methodology suggested by G. H. Junker [8].

W. D. Iwan in 1966 suggested a hysteresis model to examine the self-loosening of bolted joints and its steady state behavior. Hysteretic behavior is the characteristic of a system with regarding its past state history that is mostly observed in elastoplastic materials. Threaded fasteners are multi–body assembled structures that have both stiffness and damping characteristics. The Iwan model sketched in Figure 1.5 is structured with a distributed group of Jenkin's elements. Single Jenkin's element includes one linear spring element with the stiffness of k/N in series with a Coulomb or slip damper that has a maximum slippage limit force where the symbol N describes the total numbers of Jenkin's elements used in the Iwan model [5].

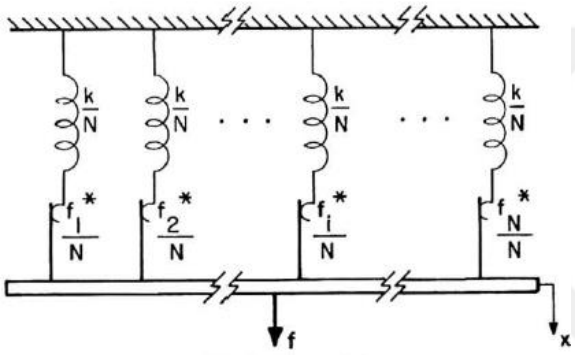

Figure 1.5 : The Iwan model with Jenkin's elements [5].

In Figure 1.6, the hysteretic plot of the system is shown in which particular elements will have limit deflection forces as described below.

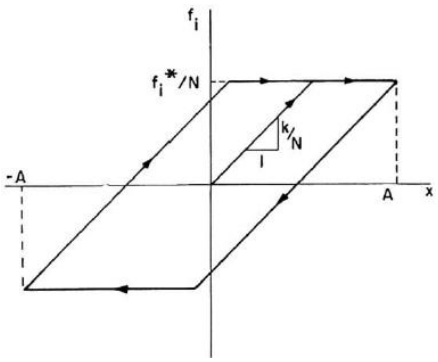

Figure 1.6 : Hysteretic behaviour

Proposed constitutive form of Iwan model can be seen in Equation 1.3 [5].

$$\boldsymbol{F(t) = \int_0^{\infty} k\tilde{\rho}\,(\tilde{\varphi})[u(t) - \tilde{x}(t,\tilde{\varphi})]d\tilde{\varphi}} \qquad (1.3)$$

Where u is the imposed displacement, F(t) is the applied force, $\tilde{\rho}(\tilde{\varphi})$ is the population density of Jenkins elements of strength $\tilde{\varphi}$, k is the stiffness common to all of the Jenkins elements, and $\tilde{x}(t,\tilde{\varphi})$ is the current displacement of sliders of strength $\tilde{\varphi}$.

In further, Segalman (2002) introduced the Four Parameter Iwan Model in order to model mechanical joints with micro slip and macro slip regions as shown in Figure 1.7. One parameter of the Iwan model is the distribution of Jenkins elements, the other parameters are of micro slip and macro slip regions [4].

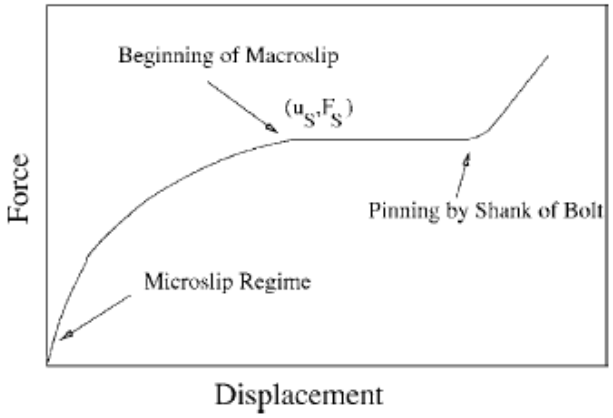

Figure 1.7 : Microslip and macroslip regions [4].

Segalman [4] proposed the Jenkins distribution function which will satisfy the modeling of distinct slip regions. In conclusion, Segalman reflected energy dissipation model of mechanical joints in derived parameters that are described in Table 1.1.

Table 1.1 : Four lap joint parameters of Iwan Model [4]

Joint Parameters	Units
Tangential stiffness (K_T)	N/m
Macroslip force (F_S)	N
Dissipation exponent (χ)	-
Stiffness ratio (β)	-

Derivation of the Iwan model joint parameters of mechanical joints requires huge number of calculations. Brake (2016) proposed the reduced Iwan model with pinning joint effect in bolted joints. In this study, due to the nature of the loading considered in washing machine components, a new Jenkins element distribution is needed for every new cycle and new loading conditions. In order to theoretically obtain

mechanical joint response, Brake suggested an assumption on reversal loading condition. If reversal loading condition were applied, distribution of Jenkins elements in other cycles would be scaled versions of original distribution. In order to evaluate an RIPP model explained in Section 2.1 with an experimental approach, the Brake–Reuß beam was used that is shown in Figure 1.8 [3].

Figure 1.8 : Brake–Reuß beam excited by shaker [3].

The Brake–Reuß beam [3] is constructed with two half steel beams. These beams are connected with three bolts within the middle region. The beam is attached with bungee cords to emulate free–free boundary conditions. An accelerometer was put at the tip of the beam. Initially, the hammer impact tests were applied in order to determine the preliminary FRFs experimentally. The bolted joints were tightened with different initial torques to observe the preload effect on the joint FRFs. In addition, the hammer impact force magnitude affects the modal behavior of the joints [2].

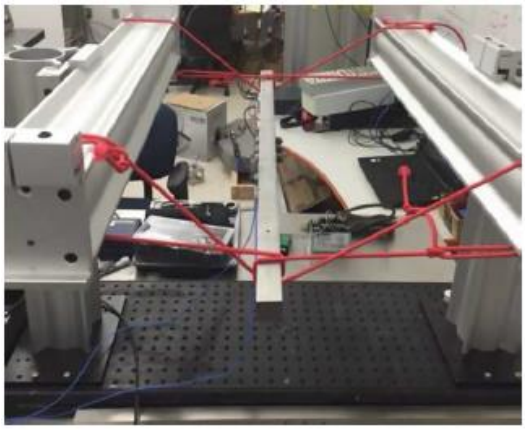

Figure 1.9 : The Brake-Reuβ beam setup [2].

Two kinds of data were recorded during the experiments such as the FRFs and time response. Time response data is used to determine the joint parameters that are mentioned below in table 1.2 with RIPP formulation [11].

Table 1.2 : Joint parameters of reduced Iwan model with pinning joint [12].

Joint Parameters	Units
Tangential stiffness (K_T)	N/m
Macroslip force (F_S)	N
Dissipation exponent (χ)	-
Stifness ratio (β)	-
Pinning Stifness (K_P)	N/m
Pinning clearance (δ_P)	mm

FRF results show that, mod frequencies are increasing with respect to initial tightening torque. In addition, inertance amplitude is increasing with proportional to tightening torque. As tightening torque increases, the pressure and contact area between parts increase as well. Thus, that results in higher joint stiffness that also increases mod frequencies [2].

Energy dissipative behavior of bolted joints are caused by the friction and contacts. Damping characteristics are also included in mating threads. One can resemble bolted joint thread damping behavior with the visco–elastically damped structures as well. Both mechanisms are strongly based on loading history and time–dependent, and they are needed to be analyzed in frequency domain. Bagley and Torvik (1983) suggested introducing fractional derivatives to below given standard linear viscoelastic structures [1],

$$\sigma(t)+\sum_{m=1}^{M} b_m \frac{d^m \sigma(t)}{dt^m} = E_0 \varepsilon(t)+\sum_{n=1}^{N} E_n \frac{d^n \varepsilon(t)}{dt^n} \tag{1.4}$$

Where σ(t) is stress history, ε(t) is strain history, t is time, M and N are number of time derivative steps, b is model parameter, E_0 is initial elasticity modulus and E_n is n^{th} step elasticity modulus. Linear viscoelastic model includes empirical parameters. Since these parameters are needed to be derived for each loading case individually, processing with this model is going to have burdensome calculations. Imposing the half derivative into linear viscoelastic equation assembles as below

$$\sigma(t)+bD^{\beta}\left\langle \sigma(t)\right\rangle = E_0 \varepsilon(t)+\mathrm{E}_1 D^{\alpha}\left\langle \varepsilon(t)\right\rangle \tag{1.5}$$

Since, fractional calculus is compatible with Laplace transform domain, Fourier transform was applied to both sides of the above equation that yields

$$\sigma^*(i\omega) + b(i\omega)^\beta = E_0\varepsilon^*(i\omega) + E_1(i\omega)^\alpha \varepsilon^*(i\omega) \tag{1.6}$$

In sum, frequency dependent modulus is a function of fractional power of frequency as follows

$$\sigma^*(i\omega) = \frac{E_0 + E_1(i\omega)^\alpha}{1 + b(i\omega)^\beta}\varepsilon^*(i\omega) \tag{1.7}$$

Where α and β are model parameters, D^α and D^β are fractional derivatives of α and β. σ*(iω) and ε*(iω) are Fourier transforms of the stress history and strain history. <..> indicates argument of operator for concerned term. Following the stiffness and damping parameters in the equation of motion can be structured and solved with Equation 1.7 [1].

1.3 Definitions in a Washing Machine

The first washing machine design was made by the German inventor Jacob Christian Schaffer in 1767. Basic principle was to mix both water and clothes in a bucket and adding rotation to increase the washing efficiency. The first design had included a manual rotating lever which provided mixing of clothes. Also, in order to dry the clothes, two rotating mandrels were used. Initial washing machine designs were in need of lots of human intervention [9].

With the technological progress through years, modern automatic front-loading washing machine was developed. As the basic principle of washing stays the same, new washing algorithms and features have been developed. With regard to that, high capacities and higher rotational speeds are demanded by customers. Manufacturers are aiming to produce high quality and cost-efficient products which are going to satisfy the customer needs with the aid of engineering. One of the most complex topics in a washing machine is to determine sufficient assembling mechanical joints which can endure life time loads and vibrations without any failure.

Washing machine cycles can be divided into two parts, washing cycle and spinning cycle. In a spinning cycle, mechanical joints are being subjected to vibrations within different frequencies. During a spinning cycle, fasteners such as screws and bolted joints may experience self–loosening failure. This failure may lead to decoupling of powertrain elements or balancing weights. Thus, loosening of any component is an undesired outcome which may harm the washing machine and disable functionality.

Figure 1.10 : Front loader washing machine.

1.4 Washing Machine Parts and Joints

Modern washing machines include a motor–belt–pulley transmission design with a rotating drum which is surrounded by a water fillable plastic or metal casing tub. A washing machine is connected to the outer body parts with springs and dampers. For machine balancing, concrete counter weights are fastened to the outer tub.

1.4.1 Motor

Generally, an automatic washing machine includes universal motor alternative current (UMAC) or brushless direct current (BLDC) motor. Output powers may vary from 450 W to 750 W. Brushless motors have higher efficiency, lower noise level and better durability than universal motors. Washing machine motors can be fastened with 2 to 4 joints mounted on the back of the oscillating tub as below, e.g., see Figures 1.11 and 1.12.

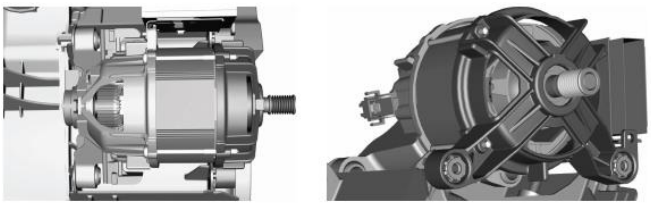

Figure 1.11 : Connection of universal motor with four joints.

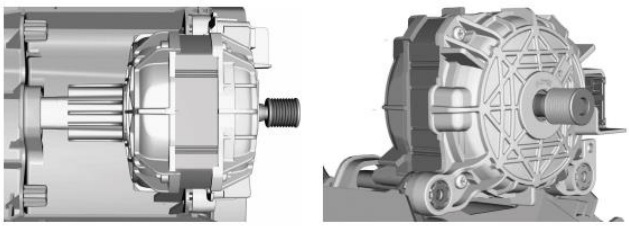

Figure 1.12 : Connection of brushless motor with two joints.

1.4.2 Belt and pulley

The belt–pulley mechanism shown in Figure 1.13 is the most common and feasible torque transmission type used in washing machines. For a pulley, its diameter is the main parameter for the transmission. The span, tension, rib type, number of ribs and friction coefficient are the significant parameters in the belt-pulley mechanism.

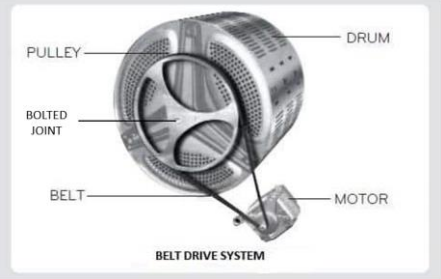

Figure 1.13 : Motor–belt–pulley transmission design.

1.4.3 Drum assembly

Drum assembly includes a shaft–flange structure which is connected to the drum with multiple threaded fasteners. The pulley and shaft are connected to each other with a preloaded axial bolted joint which is subjected to transmission torque. Parts of the drum assembly can be seen in Figure 1.14. the drum assembly is the rotor part of the washing machine. Its rotational frequency may reach up to 27 Hz.

Figure 1.14 : Parts of the drum assembly.

1.4.4 Tub assembly

In washing machines, most commonly used material for a tub is polymer. If the strength is needed due to high capacity and spin speed, polymer tubs may be reinforced with glass fibers. Plastic injection method is used for the tub production. The rear tub is being injected around the bearing house. The tub assembly is the oscillating part of a washing machine due to the unbalanced weight. The tub assembly has multiple bosses for the counter weights. The counter weights may be assembled with a direct

screw to the tub or with an inserted nut. An example assembled top counter weight can be seen in Figure 1.7.

Figure 1.15 : Tub assembly of washing machine.

Figure 1.16 : Example of top counter weight assembly.

After the drum assembly is inserted into the rear tub, the tub cover is assembled to the rear tub in order to seal the washing machine.

1.4.5 Joint types

An automatic front-loading washing machine has approximately count of 80 screws and joints on average, e.g., see Figures 1.17 and 1.18. These threaded fasteners, bolted joints etc. are being used in both dynamic group and outer body parts of the machine itself. As excitations of a washing machine arise from transmission elements and unbalanced loading amount inside the drum, all the joints are affected by the oscillating service loads.

Types of the mechanical joints in a washing machine can be divided into outer body joints and dynamic group joints. Outer body connections are very significant in the sake of determining the constraints of the outer cabinet walls, which affect modal behavior of the cabinet especially during spinning cycles.

Figure 1.17 : Counter weight screws.

It is very important to design a fitted and rigid joint for the application, since self-loosening in joints is going to result in an increase in noise level. Thus, it is focused on the group of joints attached to dynamic parts as they are experiencing higher loads and higher vibration amplitudes than those of the outer body parts. Most of the loosening failures have been detected in dynamic group joints.

Figure 1.18 : Shaft and pulley bolted joint.

1.5 Problem Definition

In mass production of washing machines, suspicious or damaged mechanical joints are checked by untightening the joints and measuring the untightening torque. Since, the preload is the most significant parameter, such actions irreversibly change the characteristic of the threaded fastener. Especially, under vibrational working conditions, checking with untightening of the joint is nearly impossible and has to be avoided.

Most important difficult task is the determination of the transferred preload through a fastener. Transferred preload plays a great role in the self-loosening mechanism of threaded fasteners. Linear static and dynamic models are not adequate since these models do not include nonlinear effects which arise from the friction. In addition, hysteresis damping characteristic of fasteners would be neglected in linear models. Former models and experiments are constructed on basic lap joints. In this study, washing machine dynamic system threaded fasteners are examined that is a complex mechanism and has a significant practical value.

1.6 Purpose of Thesis

In this study, loosening of threaded fasteners in washing machines due to vibrations is modeled and investigated with using the Reduced Iwan model with pinning joint (RIPP). The study can be divided into two parts. Firstly, identification of the model for loosening of the joints is studied theoretically and experimentally. Secondly, detection of the loosened joint is examined in frequency domain for mass production.

The reduced Iwan model with pinning joint (RIPP) model is a nonlinear modeling approach with a slider element model. Earlier studies and models are mostly conducted on lap type joints. This study covers an application of nonlinear modeling such as the RIPP model on a washing machine dynamic assembly that is a very complex structure.

In identification process, it is aimed to determine the effect of joint parameters of threaded fasteners on mechanical signature response of washing machine dynamic system. Theoretical and experimental methods are examined in parallel. For theoretical modeling, RIPP MATLAB algorithm and output measurements of the experiments are used. In experimental modeling, modal analysis of the washing machine dynamic system is completed. Then, these two models are compared with each other for verification.

In joint loosening detection process, it is needed to detect the loosened mechanical joints in mass production of washing machine for quality purposes. To this end, a detection algorithm can be implemented. Implementation process will include comparisons of experimental measurements between the tightened joints and loosened joints. In sum, experimental measurements are made and parameters of mathematical models are identified to find the loosening status if a bolted joint under static and dynamic loading conditions. Computer programs using MATLAB are developed and verified by making comparisons between their results and experimental measurements.

2. THEORETICAL MODELLING

As mentioned in the previous chapter, theoretical approaches and practical experiment designs are being studied in order to simulate and understand fastener loosening mechanisms. Bolted joints are exposed to static loads, dynamic loads and vibrations. Properly preloaded fasteners get loosened as a result of rotations as soon as relative motions occur between the mating threads and between the bearing surfaces of the fastener and clamped metal [8]. Initially, theoretical modeling of fastener loosening will be explained.

Experimentation and instrumentation are playing a vital role in order to determine loosening parameters of fasteners. Modal analysis of structures such as single degree of freedom (SDOF) and multiple degrees of freedom (MDOF) models will be explained in further. Finally, data acquisition theory and measurement system will be revisited.

2.1 Reduced Iwan Model with Pinning Joint (RIPP)

In this study, the Reduced Iwan Model with Pinning Joint (RIPP) model is going to be adapted into washing machine joints. In the RIPP model, self-loosening behavior is investigated in three specific regimes: microslip, macroslip, transition phase and pinning behavior. These distinct regimes are affected by the distribution of Iwan elements [2]. The Iwan model is constructed by the Jenkin's elements. The Jenkin's elements include a linear spring and a Coulomb friction-based slider as shown in Figure 2.1.

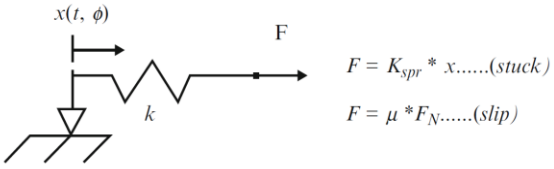

Figure 2.1 : The Jenkin's element with a linear spring and friction slider [2].

In the RIPP model, self-loosening mechanism can be modeled within three distinct regions. In distinct regions, there can be mentioned two different forces such as the Iwan force and pinning joint force that is depicted in Figure 2.2.

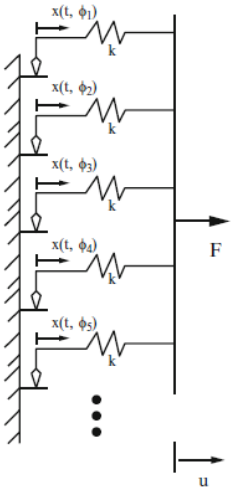

Figure 2.2 : The Iwan model with multiple Jenkin's elements [2].

Distinct regions of threaded fastener model depend on relations between relative displacements, as mentioned in Figure 2.2, and applied force to the system. These regions can be illustrated as in Figure 2.3.

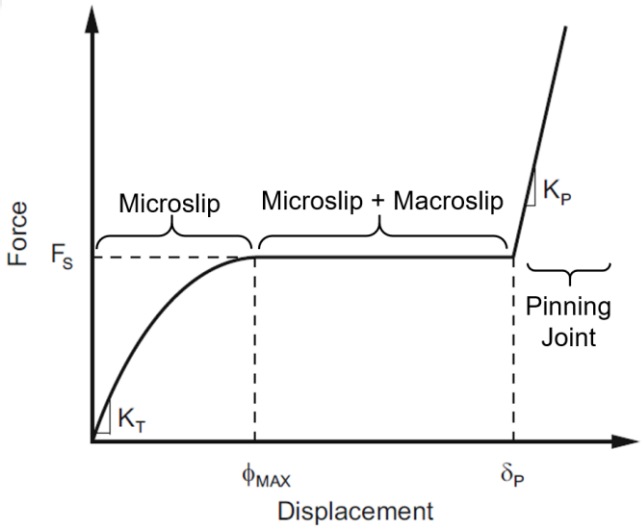

Figure 2.3 : Microslip, macroslip & pinning joint regions [2].

In microslip and macroslip regions, the Iwan force is affective. For the pinning joint phase, the pinning force will be calculated. In the microslip boundary, there is a limit displacement value, the Iwan force value and with respect to these values, a stiffness value. Within the slider effect, a relative displacement occurs even the force value does not increase. In the pinning phase, the pinning force will be effective and a pinning

stiffness parameter is introduced. Firstly, microslip and macroslip region forces and parameters will be evaluated. Secondly, pinning parameters will be evaluated.

2.1.1 Microslip and macroslip regions

Microslip and macroslip regions are exposed to nonlinear friction that is the main reason for the usage of the Iwan model. Initially, the four parameter Iwan model equation will be presented as follows [3]

$$F_{IWAN} = \int_0^{\infty} \rho(\phi)(u(t) - x(t,\phi))\,\mathrm{d}\phi \tag{2.1}$$

Where F_{IWAN} is the Iwan force, $\rho(\phi)$ is distribution of dry friction sliders which have stretched a distance, ϕ. u(t) represents global displacement and x(t, ϕ) is the relative displacements of elements. Parameter of distribution of spring–slider elements, ρ in the mechanism [2] defined by,

$$\rho(\phi) = \mathrm{R}\,\phi^{\chi}[H(\phi) - H[\phi - \phi_{\max}] + S\delta(\phi - \phi_{\max}) \tag{2.2}$$

In Equation 2.2, Heaviside function H is used for the determination of relative displacement direction. The Dirac's delta δ function determines the slider distribution with the count of S sliders in the modeled threaded fastener. S and other expressions besides functions and displacement variable ϕ are fastener parameters that can be delivered experimentally. Above experimental parameters are often transformed into another pack of physical parameters such as F_s, K_T, β and χ.

For the Iwan Force F_s, every Iwan model element is considered to be sliding. In Equation 2.1, the displacement term will be ϕ. Thus, Equation 2.1 becomes

$$F_S = \int_0^{\infty} \rho(\phi)\phi\,\mathrm{d}\phi \tag{2.3}$$

For the stiffness parameter, the displacement ϕ will vanish from Equation 2.3 as follows

$$K_S = \int_0^{\infty} \rho(\phi)\,\mathrm{d}\phi \tag{2.4}$$

In order to determine the Iwan force in the macroslip region behavior, Equation 2.2 is going to be substitute into (2.3). Then,

$$F_s = \frac{R\phi_{\max}^{\chi+2}}{\chi+2} + S\phi_{\max} \tag{2.5}$$

In the above Equation 2.5, a new parameter β is going to be introduced. This new parameter will be dimensionless. In further, β will be corresponding to a stiffness ratio with respect to energy dissipation of the joint. A representative plot will be energy dissipation amount with regards to occurred displacement within applied force [5] as follows

$$\beta = S \Big/ \left(\frac{R\phi_{\max}^{\chi+1}}{\chi+1} \right) \tag{2.6}$$

Within the definition of β, Equation 2.5 can be expressed as follows

$$F_s = \phi_{\max} \left(\frac{R\phi_{\max}^{\chi+1}}{\chi+1} \right) \left[\frac{\chi+1}{\chi+2} + \beta \right] \tag{2.7}$$

For further calculations, S and R terms will be expressed with the four parameters of the Iwan model. One can derive term R from Equation 2.7. Also, the parameter S can be derived from both Equations 2.6 and 2.7. Then,

$$R = \frac{F_S(\chi+1)}{\phi_{\max}^{\chi+2} \left(\beta + \frac{\chi+1}{\chi+2} \right)} \tag{2.8}$$

$$S = \left(\frac{F_s}{\phi_{\max}} \right) \left(\frac{\beta}{\beta + \left(\frac{\chi+1}{\chi+2} \right)} \right) \tag{2.9}$$

In conclusion, all mathematical model parameters are converted into physical parameters [2].

As F_S is determined, microslip region force F_{IWAN} in Equation 2.1 needs to be calculated. In the Jenkin's elements, two conditions are observed, stuck slider and sliding slider, as stated in Figure (2.1). This brings a new function definition of sliding occurrence as follows

$$\Gamma(u,\phi) = u - x(t,\phi) = \begin{cases} u & \text{if stuck slider } u < \phi \\ \phi & \text{if sliding slider } u \geq \phi \end{cases} \tag{2.10}$$

One can substitute the sliding function in Equation 2.1. Then, we get

$$F_{IWAN} = \int_0^{\phi_{\max}} \Gamma(u,\phi) R\phi^{\chi} d\phi + S\Gamma(u,\phi_{\max}) \tag{2.11}$$

Since, Γ function has both conditions, above integral may be separated into two different parts.

$$F_{IWAN} = \int_0^{u} R\phi^{\chi+1} d\phi + \int_u^{\phi_{\max}} uR\phi^{\chi} d\phi + S\Gamma(u,\phi_{\max}) \tag{2.12}$$

Solution of the above integral will be as follows

$$F_{IWAN} = R\left(\left(\frac{1}{\chi+2} - \frac{1}{\chi+1}\right)u^{\chi+2} + \frac{\phi_{\max}^{\chi+1}}{\chi+1}u\right) + S\Gamma(u,\phi_{\max}) \tag{2.13}$$

As mathematical parameters, *R* and *S* have been transitioned into physical parameters and these will be substituted into Equation 2.13. Hence, the four parameter Iwan Force will be determined as follows

$$F_{IWAN} = \frac{F_S(\chi+1)}{\phi_{\max}^{\chi+2}\left(\beta + \frac{\chi+1}{\chi+2}\right)} * \left(\left(\frac{1}{\chi+2} - \frac{1}{\chi+1}\right)u^{\chi+2} + \frac{\phi_{\max}^{\chi+1}}{\chi+1}u\right) + \left(\frac{F_s}{\phi_{\max}}\right)\left(\frac{\beta}{\beta + \left(\frac{\chi+1}{\chi+2}\right)}\right)\Gamma(u,\phi_{\max}) \tag{2.14}$$

2.1.2 Pinning region

The pinning force occurs when two cylindrical faces of bolt shaft and inside of screw hole interact with each other. In such a contact, this can be identified as Hertz's elastic contact model whether no plastic deformation occurs [3].

For a bolt shaft and screw hole, cylindrical Hertz contact force will be used given by the below equation

$$F_{PINNING} = \frac{\pi}{4} E^* L d \tag{2.15}$$

where E^* represents the effective contact elastic modulus, L is the length of contact and d is the contact interference that can be expressed by the displacement ϕ and bolt radius δ_p as follows

$$d = \phi - \delta_p \tag{2.16}$$

The two surfaces also will have the Poisson's ratios of v_1 and v_2. Hence, effective elastic modulus will be determined as follows

$$E^* = \left(\frac{1-\nu_1^2}{E_1} + \frac{1-\nu_2^2}{E_2} \right) \tag{2.17}$$

Since the contact force is elastic and linear, the pinning stiffness can be expressed as below

$$K_P = \frac{\pi}{4} E^* L \tag{2.18}$$

In order to reflect the pinning force to the system correctly, the pinning force will be expressed with the Heaviside step function as it is determined to be in the situation of bolt shaft and screw hole contact as follows

$$F_{PINNING} = \pm H(\delta_0 \pm u \mp \delta_P) * K_P(\delta_0 \pm u \mp \delta_P) \tag{2.19}$$

In conclusion, all of the Iwan parameters and effective forces are expressed.

2.2 Implementation of RIPP Joint Algorithm

In an experimental system, measured acceleration data will be submitted to an RIPP joint algorithm. It is aimed at deriving the hysteresis behavior and determine effect of joint parameters [2]. A sample algorithm can be found in [12]. Data in time domain is being inserted as input data.

2.3 Theory of Modal Analysis

Modal analysis and modal testing methods are expanding their application areas in the prospect of mechanical signal response of various structures. Modal analysis visualizes the response of a structure under dynamic conditions. In order to properly develop a

comprehension of theory, one needs to acknowledge that there are three different models of a structure in the basis of vibrational analyses.

Spatial model is the mathematical model that determines the stiffness and damping characteristics and inertia of a structure [13] whose equation of motion is expressed by

$$m\ddot{x} + c\dot{x} + kx = 0 \tag{2.20}$$

Modal model defines the signature behavior of the structure within vibration modes and mode shapes, algebraically eigenvalues $\bar{\omega}_r^2$ and eigenvectors Φ without any external interference. Every structure has its own unique modal model that is only expressed with natural frequency and mode shape parameters. There is an algebraic relation between spatial model and modal model as below [13]

$$\Phi^T m \Phi = I \tag{2.21}$$

$$\Phi^T k \Phi = \bar{\omega}_r^2 \tag{2.22}$$

The response model includes an input/output relationship from a specific unique excitation. Input/output ratio is called frequency response function (FRF) and designated as $H_{jk}(\omega)$. For a proper response function, it is obligated to have a single excitation. Mechanical systems or structures may have responses within defined degrees of freedom.

$$H_{jk}(\omega) = \left(\frac{X_j}{F_k} \right) \tag{2.23}$$

The response model also has a relationship between both spatial model and modal model [13] as follows

$$H(\omega) = (k - \omega^2 m)^{-1} = \Phi \left[(\bar{\omega}_r^2 - \omega^2) \right]^{-1} \Phi^T \tag{2.24}$$

2.3.1 Single degree freedom Modal Analysis

In mechanical systems, most of the models are subdivided and modeled as an SDOF system as depicted in Figure 2.4. Modeling as a SDOF system is significant since multi body and multi degrees of freedom structures can be modeled as the superposition of SDOF models. The SDOF models can be divided into three sub topics.

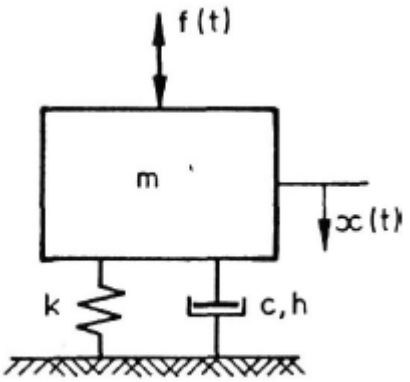

Figure 2.4 : Representation of SDOF systems [14].

Undamped SDOF systems consist of a mass and spring. For modal model, there will be no force excitation. In further calculations, the implementation is going to be based on the modal equation of motion (2.20) with a harmonic motion assumption of $x(t) = Xe^{i\omega t}$. Hence, below given frequency response function is determined [14]

$$H(\omega) = \frac{X}{F} = \frac{1}{(k - \omega^2 m)} \tag{2.25}$$

Viscously damped systems are represented with a dashpot coefficient of c in the equation of motion (2.20). In modal solution of (2.20), it will include a complex single natural frequency with real and imaginary parts. The imaginary part is known as the oscillatory part while the real part is known as the decaying part, e.g., see Figure 2.5.

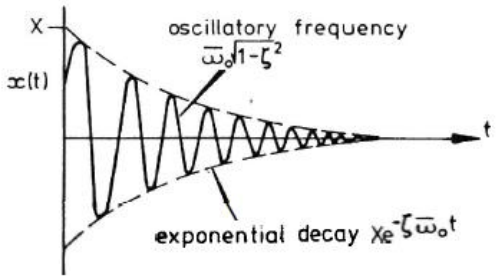

Figure 2.5 : Oscillatory frequency and exponential decay.

In sum, frequency response function can be determined with real and imaginary parts. The magnitude and phase of the modal response can be also derived from FRF given by

$$H(\omega) = \frac{X}{F} = \frac{1}{(k - \omega^2 m) + i(\omega c)} \tag{2.26}$$

Damped structural systems do not include a constant damping value within differentiated mod frequencies. That is the reason that a dashpot does not satisfy a real damping model. Damping definition is energy dissipation per cycle over maximum stored energy [14]. Structural damping can be divided into material hysteresis and dry friction. Force displacement representation of damping models can be seen in Figure 2.6

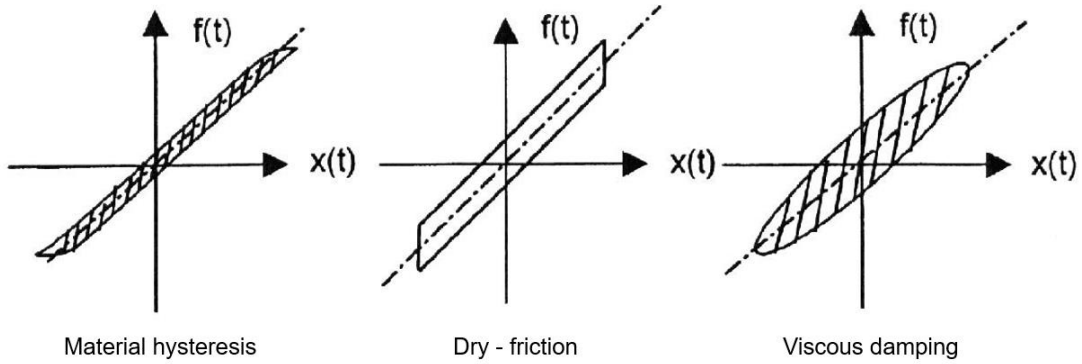

Figure 2.6 : Force displacement plots of different damping models.

Frequency response function of structurally damped models include a damping loss factor of η and it replaces critical damping ratio term in viscously damped FRF given by Equation 2.26. That is,

$$H(\omega) = \frac{X}{F} = \frac{1/k}{(1-(\omega/\bar{\omega}_0)^2 + i\eta)} \tag{2.27}$$

A sample FRF plot of accelerance can be seen in Figure 2.7

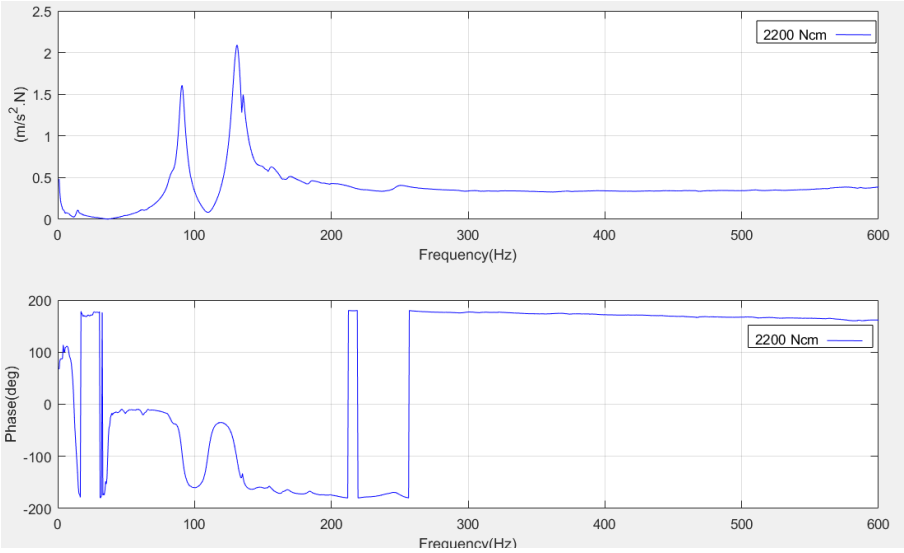

Figure 2.7 : Magnitude and phase curves of a sample accelerance FRF plot.

2.3.2 Multi degree freedom Modal Analysis

Real mechanical structures have multiple degrees of freedom, e.g., see Figure 2.8. Mass, stiffness and damping coefficients are going to be a combination of each degree of freedom (DOF). Hence, these properties will be represented as matrices and vectors. Then, governing equation of motion for undamped systems having *N* DOF can be expressed as follows

$$[M]\{\ddot{x}(t)\}+[K]\{x(t)\}=\{f(t)\} \tag{2.28}$$

where mass [*M*] and stiffness [*K*] are the matrices having the size *N*x*N*. Also, {*x(t)*} and {*f(t)*} are the vectors having the size of *N*x1. In order to solve the governing equation of motion, free vibrations will be determined initially to obtain the homogenous solution with the assumption of {*f(t)*} = {*0*}.

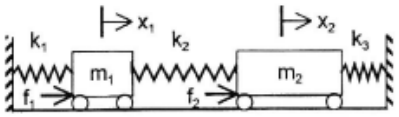

Figure 2.8 : A sample multi degrees of freedom system [14].

Solution of harmonic motion, $\{x(t)\} = \{X\}e^{i\omega t}$ will lead to the below equation

$$\left([K]-\omega^2[M]\right)\{X\}e^{i\omega t}=\{0\} \tag{2.29}$$

Nontrivial solution condition of Equation 2.29 is as follows

$$\det\left|[K]-\omega^2[M]\right|=0 \tag{2.30}$$

that gives the natural frequencies of *N* DOF via the eigenvalue solution. If one substitutes the natural frequency of a specific DOF in Equation 2.30, corresponding eigenvector solution will give the associated mode shape. The complete solution of natural frequencies will be in the form of $\left[\ddots\bar{\omega}_r^2\ddots\right]$ and the mode shapes will be formed of a matrix $[\psi]$ having the eigenvectors in columns. The corresponding r^{th} natural frequency will address to the r^{th} mode shape.

In modal model of MDOF systems, orthogonality is an important property. Orthogonality introduces mass normalized mode shapes as below [14]

$$[\psi]^T[M][\psi]=[m_r] \tag{2.31}$$

$$[\psi]^T [K][\psi] = [k_r] \tag{2.32}$$

In Equations 2.31 and 2.32, $[m_r]$ and $[k_r]$ refer to modal mass and modal stiffness of the r^{th} mode, respectively. The frequency response function $[H(\omega)]$ of MDOF undamped systems can be expressed as follows

$$[H(\omega)] = \frac{\{X\}}{\{F\}} = \left([K] - \omega^2[M]\right)^{-1} \tag{2.33}$$

Using Equations 2.31 and 2.32 along with the orthogonality property, the FRF will be determined with modal mass and modal stiffness as follows

$$H_{jk}(\omega) = \sum_{r=1}^{N} \frac{\left(\psi_{jr}\right)\left(\psi_{kr}\right)}{m_r\left(\bar{\omega}_r^2 - \omega^2\right)} \tag{2.34}$$

For proportionally damped MDOF systems, below given frequency response function is determined

$$[H(\omega)] = \frac{\{X\}}{\{F\}} = \left([K] + \mathrm{i}\,\omega[C] - \omega^2[M]\right)^{-1} \tag{2.35}$$

where damping matrix can be assumed to be proportional to stiffness matrix as $[C] = \beta[K]$, i.e., Rayleigh damping model. Following, proportional damping matrix $[C]$ will be employed. In brief, following Equation 2.34, the below given FRF equation can be derived

$$H_{jk}(\omega) = \sum_{r=1}^{N} \frac{\left(\psi_{jr}\right)\left(\psi_{kr}\right)}{\left(k_r - \omega^2 m_r\right) + i\left(\omega c_r\right)} \tag{2.36}$$

where modal damping term is represented by c_r.

As mentioned in SDOF systems, hysteresis damping can be introduced with proportional damping in the following form $[D] = \beta[K] + \gamma[\mathrm{M}]$. Following, damping loss factor is introduced as follows

$$\eta_r = \beta + \gamma / \bar{\omega}_r^2 \tag{2.37}$$

Hence, the corresponding FRF becomes similar to that of a SDOF system. Two alternative representations of the FRF for MDOF systems can be expresses as follows [14]

$$H_{jk}(\omega) = \sum_{r=1}^{N} \frac{\left(\psi_{jr}\right)\left(\psi_{kr}\right)}{\left(k_r - \omega^2 m_r\right) + i\eta_r k_r} \tag{2.38}$$

$$H_{jk}(\omega) = \sum_{r=1}^{N} \frac{\left(\psi_{jr}\right)\left(\psi_{kr}\right)}{m_r(\omega_r^2 - \omega^2 + i\eta_r\omega_r^2)} \tag{2.39}$$

2.4 Data Acquisition

Signal processing and data acquisition are the vital steps for the modal analysis and modal testing. Initially, if any sensor system will be embedded to a system, the engineers shall acknowledge how an analog output is collected and converted into a digital signal. In order to guarantee the validity of measurement, one needs to justify the trustworthiness of data. Output data may be erroneous in the possibility of aliasing or leakage.

Aliasing occurs when sampling frequency of data acquisition system is lower than the frequency content of measured signal. To prevent aliasing, there are basic filters need to be applied which is called anti–aliased filters. Hence, sampling frequency of the system is significant. An example of aliasing can be seen in Figure 2.9.

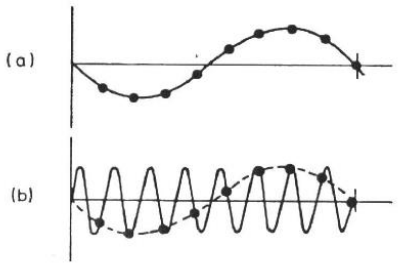

Figure 2.9 : Aliasing example, (a) is sampled signal, (b) is original signal with sampled signal [14].

Leakage is an error which is arising when analyzed signal is not periodic. Leakage error can be corrected with applying windowing such as the Hanning window that is widely used in practice. A sample application can be seen in Figure 2.10 [15].

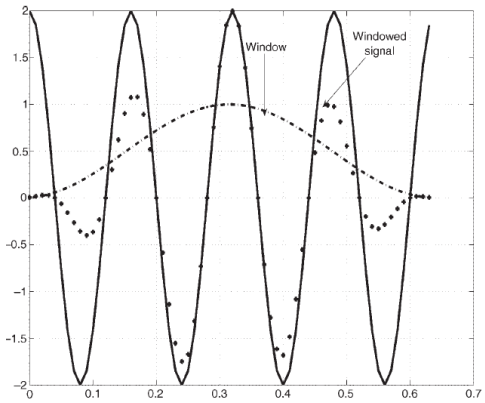

Figure 2.10 : Application of Hanning windowing to a time domain signal [15]

In modal analysis, collected time domain data is transformed into frequency domain with Fourier transform. Most signal analyzers are using Fast Fourier Transform (FFT) and provide direct measurement of FRFs [13]. Exponential form of Fourier series can be found below [15]

$$X_k = \frac{1}{T}\int_T x(t)\exp(-j2\pi k f_0 t)dt \tag{2.40}$$

A sample multichannel FFT analyzer can be seen in Figure 2.11.

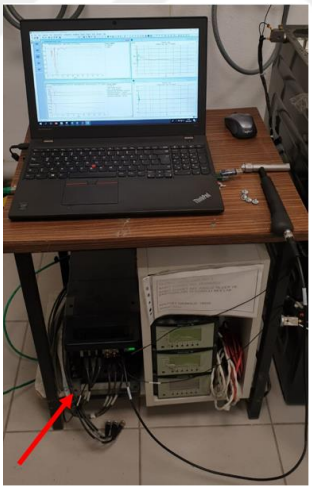

Figure 2.11 : Multichannel FFT analyzer (bottom left) used in a hammer impact test.

3. EXPERIMENTAL MODELLING

In order to obtain dynamic model of threaded fasteners, two different experiment types were conducted. As mentioned earlier, one of the important parameters of bolted joints is tightening torque and preload.

First mentioned experiment will be modal testing. Impact hammer experiments were performed in order to identify loosening joints via natural frequencies, phase variations and mod shapes. Secondly, with the excitation of a shaker, preload behavior of threaded fasteners was examined. Also, relative motion between the bolts and nuts were determined in order to determine microslip and macroslip behaviors.

3.1 Impact Hammer Test

Purpose of the impact hammer test shown in Figure 3.1 is to identify loosening behavior. In this experiment, modal analysis tools and equipment were used [16]. Test procedure is to excite the tub from various points with an impact hammer and to measure accelerations on threaded fasteners. Excited washing machine was in the condition of statically standing.

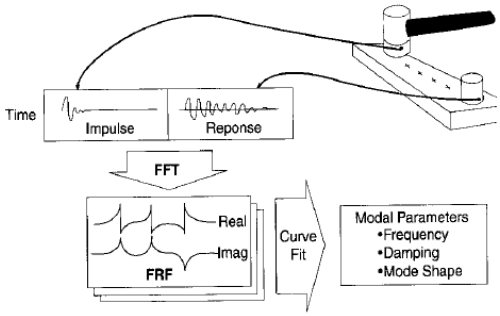

Figure 3.1 : A brief illustration of impact hammer test [16].

It is aimed at identifying loosening modeling of a washing machine top counter weight threaded fasteners. As mentioned earlier, counterweights are mounted with multiple joints as in this experiment including three threaded fasteners. A sample section view of counter weight assembly can be seen in Figure 3.2.

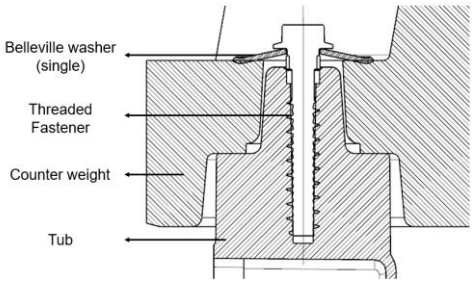

Figure 3.2 : A sample section view of washing machine counter weight assembly.

3.1.1 Procedure of experiment

Initially, excitation points and measurement points on the test sample are determined. Furthermore, an accelerometer was placed at measurement points and impact excitation was applied. The excitation was applied to the tub, fastener and counterweight. As measurements are examined, it is decided that excitation from the tub and acceleration measurements at counter fasteners will be characterizing the force transmission very accurately. In Figure 3.3, the numbers 1, 2, 3, 4, 5 and 6 indicate the impact hammer excitation points on the tub. Measurements points are indicated by the letters as A, B and C and the sensor is placed on the head of the threaded fastener.

Figure 3.3 : Excitation points are denoted by numbers and measurement points are denoted by letters.

Experiments were repeated and measurements were recorded. Purpose of the test is to identify the changes in modal characteristics such as variations in mode frequencies, amplitudes and phase angles.

3.1.2 Experimental setup

In this section, the tools and equipment used in experiments are introduced and explained. In these tests, the impact hammer was the Bruel & Kjaer Type 8206, as can be seen in Figure 3.4. This impact hammer is well fitted for impact force measurements on small to medium structures, measurement of FRFs using impact excitation methods

and estimation of structural response characteristics as a part of dynamic structural testing.

Figure 3.4 : Impact hammer B&K Type 8206 used in the experiments.

As a measurement sensor, the accelerometer Bruel and Kjaer Type 4397 was used. The sensor is shown in Figure 3.5. The sensor B&K Type 4307 is a fitted choice since threaded fastener critical frequencies are in the range of medium and high frequencies.

Figure 3.5 : Accelerometer B&K Type 4397 used in the experiments.

For data recording and analyzing, a PC with the software named PULSE Labshop is used. In the software, force and acceleration data in time domain, frequency response function of excitations, coherence, measured data continuity and quality are extracted. Also, a multi-channel analyzer is used for signal analyses. This setup can be seen in Figure 3.6.

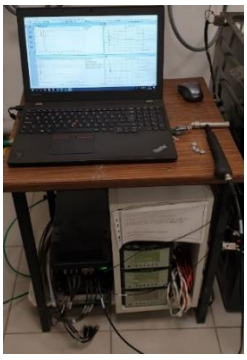

Figure 3.6 : Data recorder and analyzer.

3.2 Identification with Impact Hammer Test

3.2.1 Determination of transmissibility

Before starting the measurements, an experiment plan given in Table 3.1 was prepared. The main objective was to determine the threaded fasteners which show high distinction effect of loosening.

Table 3.1 : Experimental plan for impact hammer tests.

Exp #	Tightening Torque (N.cm)			Excitation Matrix			
	Screw A	Screw B	Screw C		Screw A	Screw B	Screw C
Exp1	2200	2200	2200	Tub1	1	7	13
Exp2	2000	2200	2200	Tub2	2	8	14
Exp3	1800	2200	2200	Tub3	3	9	15
Exp4	1600	2200	2200	Tub4	4	10	16
Exp5	1400	2200	2200	Tub5	5	11	17
Exp6	1200	2200	2200	Tub6	6	12	18
.	.	.	.	.	.	.	.
.	.	.	.	.	.	.	.
.	.	.	.	.	.	.	.

In order to get adequate data about the status of mechanical joints, a test sample is excited differently. Different response points were compared at the beginning. Two different scenarios were followed. Firstly, an accelerometer was placed on the center of mass of counter weight. In the second scenario, an accelerometer was placed on the untightened Screw A. In both scenarios, tightening torques at Screw B and Screw C were at maximum value of 2200 Ncm. The torque at Screw A was at 200 Ncm. Furthermore, excitation point on the tub was the same point as T1. Comparisons of FRFs can be seen in Figure 3.7. In conclusion, taking the response from the head of the screws were more adequate in the perspective of FRF amplitudes in identification of loosening of bolts.

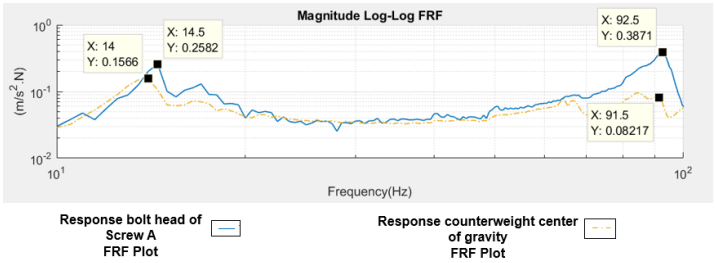

Figure 3.7 : FRF plots from different response points.

For the purpose of identifying the loosening behavior of bolted joints, comparisons of responses were made among the fully tightened, tightened with the torque of 2200 Ncm and a reduced tightening torque of 200 Ncm. In Table 3.2, the torque values of the screws can be seen.

Table 3.2 : Torque values used in experiments for loosening determination.

	Torque (N.cm)
Screw A	200
Screw B	2200
Screw C	2200

It was aimed at deriving how force transmissibility is affected though a stiff or loosened connection. In resulting FRF plots of acceleration measurements shown in Figure 3.8, the FRF amplitude values of a loosened screw were larger than those of the tightened screw. Another point is that loosened joint FRF amplitudes were being lowered as moving away from the joint itself.

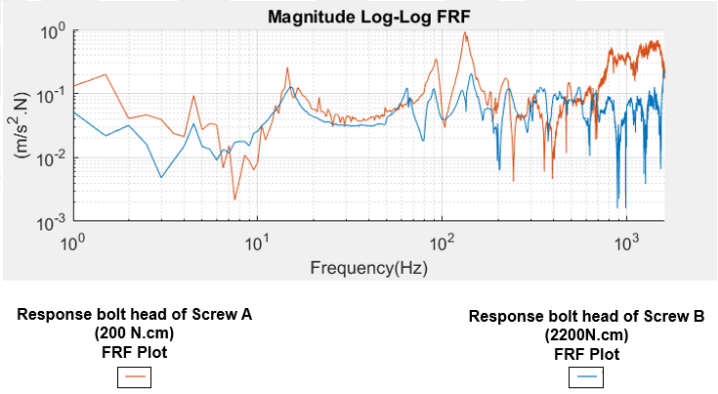

Figure 3.8 : The FRF plots of the reference point for a high torque and low torque.

Additional reciprocity checks of loosening identification were made to determine the high stiffness along the excitation direction. In this scenario, torque values can be seen in Table 3.3.

Table 3.3 : Torque values loosening determination in scenario #2.

	Torque (N.cm)
Screw A	2200
Screw B	2200
Screw C	200

It was determined that the response of the loosened mechanical joint's acceleration amplitude is deliberately larger than that of the tightened joints. Furthermore, due to

loosening, non-linear behavior was examined. In Figure 3.9, an anti-resonance point was observed at 33 Hz. Taking measurements at different points helped conclude that data which was taken from a loosened joint was more decisive.

As from phase perspective, connection stiffness of measured point is affecting the phase shift. At lower frequencies, phase response from stiffener joint is more regular rather than low stiff joint. At higher frequencies response from loosened joint is more stable since impact point has higher torque value. In reciprocity check, phase shift $\pm\pi/2$ is observed.

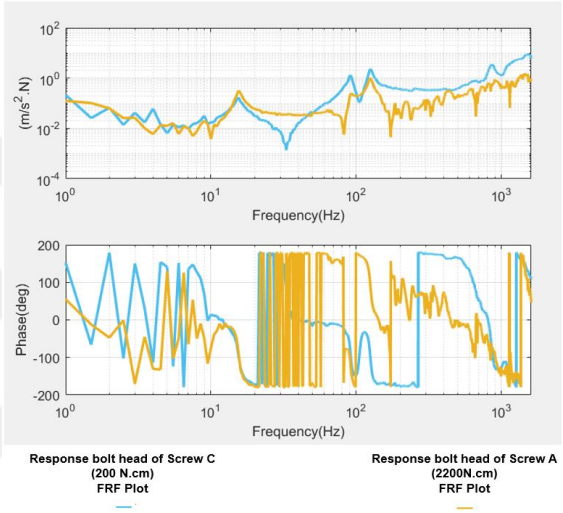

Figure 3.9 : Reciprocity check between loosened joint and normal joint.

As experiments proceeded following the Table 3.4, primary aim was to identify the excitation and measurement points which reflect good quality of force transmissibility and acceleration. Initial measurements taken from different regions are shown in below given Table 3.4.

Table 3.4 : Various measurements with high and low tightening torques.

Excitation Point	Measurement Point	Torque A	Torque B	Torque C	Mode (Hz)	Amplitude (m/s^2.N)
Tub-1	Screw-A	1600	2000	2000	14.5	1.39E-01
Tub-1	Screw-A	1600	2000	2000	92	3.72E-01
Tub-1	Screw-A	1600	2000	2000	133	9.87E-01
Tub-1	Screw-A	1600	2000	2000	135.5	8.39E-01
Tub-1	Screw-A	1600	2000	2000	225	1.68E-01
Tub-1	Screw-A	400	2000	2000	14.5	2.58E-01
Tub-1	Screw-A	400	2000	2000	17	1.30E-01
Tub-1	Screw-A	400	2000	2000	93.5	3.47E-01
Tub-1	Screw-A	400	2000	2000	133	9.67E-01
Tub-1	Screw-A	400	2000	2000	136	8.58E-01
Tub-1	Screw-A	400	2000	2000	225	1.75E-01
Tub-4	Screw-B	2200	2000	2200	14.5	1.47E-01
Tub-4	Screw-B	2200	2000	2200	83.5	4.20E-01
Tub-4	Screw-B	2200	2000	2200	146	5.65E-01
Tub-4	Screw-B	2200	1000	2200	15	1.40E-01
Tub-4	Screw-B	2200	1000	2200	83	4.30E-01
Tub-4	Screw-B	2200	1000	2200	144.5	5.94E-01
Tub-5	Screw-C	2200	2200	2200	14.5	1.07E-01
Tub-5	Screw-C	2200	2200	2200	91	1.61E+00
Tub-5	Screw-C	2200	2200	2200	131	2.09E+00
Tub-5	Screw-C	2200	2200	2200	783	4.05E-01
Tub-5	Screw-C	2200	2200	2200	1190	6.33E-01
Tub-5	Screw-C	2200	2200	200	15.5	1.73E-01
Tub-5	Screw-C	2200	2200	200	91	1.32E+00
Tub-5	Screw-C	2200	2200	200	125.5	2.29E+00
Tub-5	Screw-C	2200	2200	200	861	3.50E+00
Tub-5	Screw-C	2200	2200	200	1559	8.72E+00

These results pointed out that excitation on the of point Tub-5 and measuring from Screw C was going to provide results that can be utilized further. Other measurements were not able to provide wide frequency examination knowledge since data quality and transmissibility were not adequate. The reason behind the selection of points Tub-5 and Screw C is that the excitation and response point distance were closer than the other points. That is also depending on nonlinearity of the subject. Furthermore, the chosen points' transmissibility in high frequencies are better than that of the other points, which can be seen in Figure 3.10.

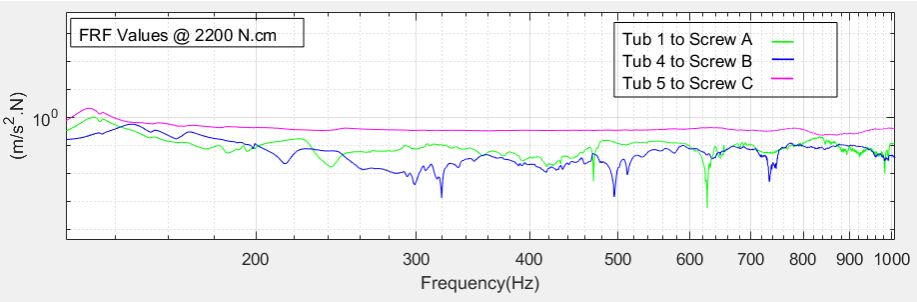

Figure 3.10 : Force transmissibility of point pairs in high frequency range.

3.2.2 Determination torque effect on frequency response

To determine the optimal points to be used in experiments, the FRFs were calculated for varying torque of a single threaded fastener. In the following plots, distinctive behavior with changing tightening value will be explained.

In Figure 3.11, the entire FRF magnitude and phase plots for the tightening torques of 2200 Ncm, 2000 Ncm and 200N.cm can be seen.

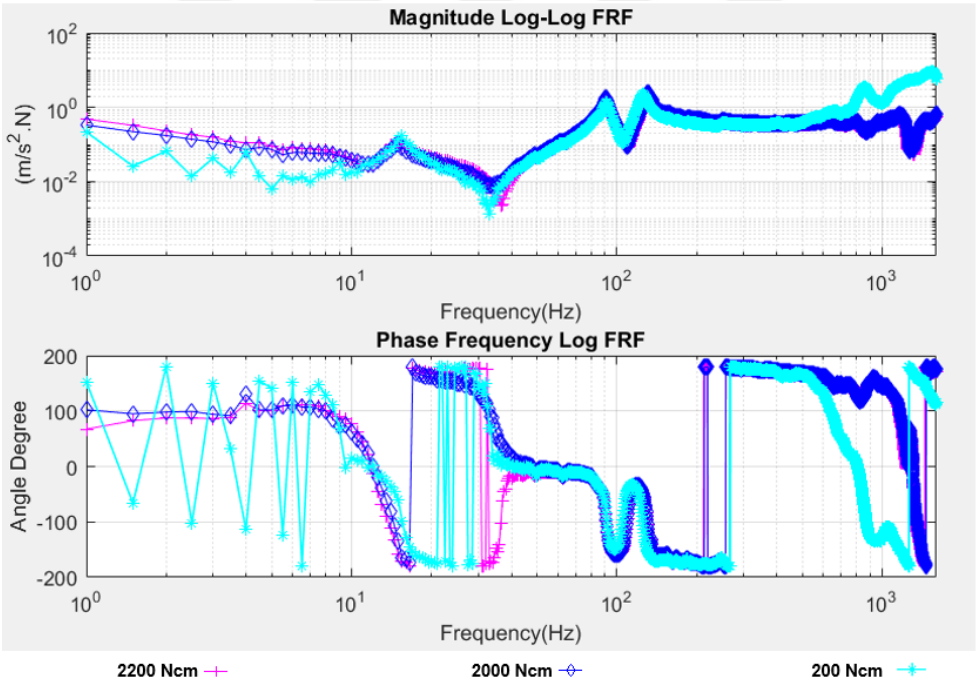

Figure 3.11 : FRF plots for the tightening torques of 2200 Ncm, 2000 Ncm and 200 Ncm.

At lower torque value, macroslip behavior is being more effective and significant phase disturbance is observed. Phase identity of 2200 Ncm is shifted amount of $\pm\pi/2$ at 2000 N.cm and 200 Ncm. Phase shift initiation indicates beginning of microslip and macroslip behavior between 10 Hz and 100 Hz.

At low frequencies such as 1 to 10 Hz range, the behavior of the joint for the high torque values such as 2200 Ncm and 2000 Ncm were more stiffer than that of the low torque value of 200 N.cm. As tightening torque reduces, nonlinear damping effect increases. Furthermore, immediate phase changes were observed. In Figure 3.12, the FRF plots in the frequency range of 1-10 Hz can be seen.

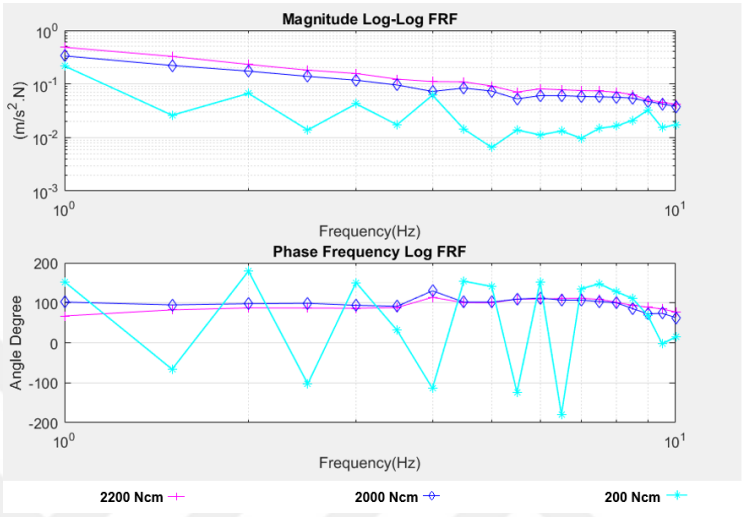

Figure 3.12 : FRF plot in low frequencies in the range of 1 to 10 Hz.

In Figures 3.11 and Figure 3.12, nonlinear behavior in joints was graphically identified. It is aimed at finding for which torque value is the limit that nonlinear behavior begins. For the tightening torques of 1800 Ncm and below, FRF plot characteristics are similar in low frequencies. This similarity can be seen in Figure 3.13.

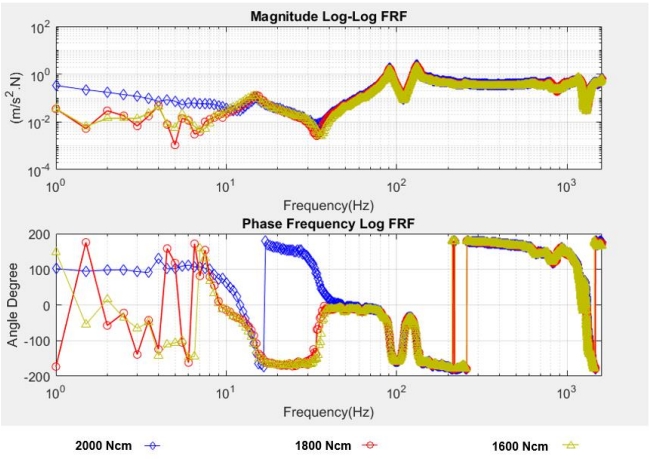

Figure 3.13 : FRF plots for the tightening torques of 2000 Ncm, 1800 Ncm and 1600 Ncm.

Nonlinearity in 1800 Hz is pointing out the occurrence of microslip and macroslip behavior in the frequency range of 1 to 10 Hz. For slightly higher frequencies such as

the frequency range of 20 to 30 Hz, the tightening torque of 600 Ncm is the quite limit for the behavior of nonlinearity region. In Figure 3.14, higher tightening torques have flat phase angle, although, tightening torque of 600 Ncm has prompt phase angle changes. Between 10 Hz – 100Hz identical phase variation of ±π/2 is observed between 2000 Ncm and decreased torque values, 1800 Ncm – 1600 Ncm.

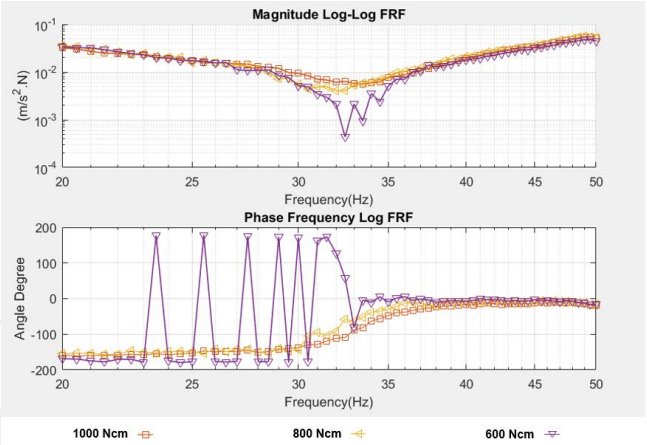

Figure 3.14 : FRF plots for the tightening torques of 1000 Ncm, 800 Ncm and 600 Ncm.

In Figure 3.14, the discrepancy between the tightening torque of 600 Ncm and higher torques continues up to 35 Hz. At 32.5 Hz, the tightening torque of 600 Ncm has an anti-resonance behavior which indicates that force transmissibility is reduced due to damping effect. Damping effect at 600 Ncm torque value also can be seen in phase plot. At 33 Hz of 600 Ncm, phase shift of π/2 occurs. Phase shift of π/2 means that macroslip effect causes delay on transmitting the act force itself. On the other hand, π/2 phase shift is not seen at 800 Ncm and 1000 Ncm in Figure 3.14 which implicates connection at these torque values are stiffener than 600 Ncm.

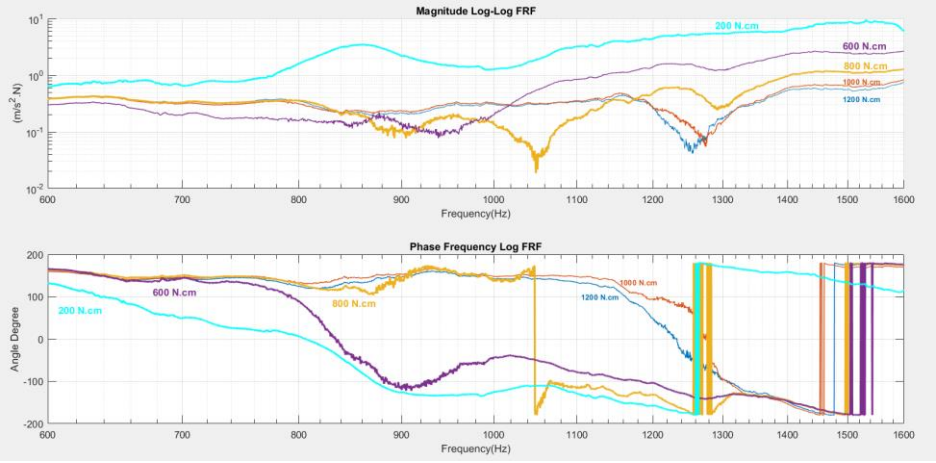

Figure 3.15 : FRF plots for the tightening torque of 1200 Ncm, 1000 Ncm, 800 Ncm, 600 Ncm and 200 Ncm.

In more elevated frequencies such as 600 Hz to 1600 Hz, the tightening torque of 800 Ncm is the limit torque value that two types of behavior can be seen as shown in Figure 3.15. It is predicted that at such a high frequency, microslip to macroslip regions are occurring. In Figure 3.15, the tightening torque of 800 N.cm in the joint results in microslip condition until a cut-off frequency of 1050 Hz. As indicated in Figure 3.15, an anti–resonance behavior occurs at 1050 Hz, which leads to nonlinearity. The characteristic of the tightening torques above 800 Ncm and below 800 Ncm is quite different.

In sum, consolidated results show that the maximum four modes appear in high torque values. On the other hand, for the tightening torques of 600 Ncm and 800 Ncm, the 5^{th} modes also observed in experimental measurements. As the tightening torque is lowered, the 4^{th} mode frequency decreases since the bolt contacts are decoupled and stiffness of the connection is diminishing. For lower tightening torque values, the behavior of macroslip region is triggering higher modes to be observed in measurements. Loosening of joints does not affect the 1^{st} and 2^{nd} mode frequencies. The reason behind is that macroslip and microslip behavior is not affected; thus, connection amplitudes are not affected. In 200 Ncm condition, 3^{rd} mode frequency is significantly affected and decreased to 125 Hz, on the other hand, for other tightening torque values, the 3^{rd} mode frequency is slightly affected around ± 1.5 Hz. Tabular forms of identification measurements can be seen in Tables 3.5 and 3.6.

It should be noted that, all phase shifts are also arising from microslip and macroslip effects related to tightening torque value degradation. Especially, lower torque values make the connections less stiff and damping characteristics being more effective which lead to phase shifts.

Table 3.5 : Mode frequencies in Hz for different tightening torques.

			Torque value of C									
Excitation Point	**Measurement Point**	**Mode**	**200 N.cm**	**600 N.cm**	**800 N.cm**	**1000 N.cm**	**1200 N.cm**	**1400 N.cm**	**1600 N.cm**	**1800 N.cm**	**2000 N.cm**	**2200 N.cm**
Tub-5	**Screw-C**	**Mode#1(Hz)**	15.5	15.5	15.5	14.5	15.0	14.5	14.5	15.0	15.0	15.0
		Mode#2(Hz)	91.5	91.0	91.5	91.0	91.0	91.0	91.0	91.0	91.0	91.0
		Mode#3(Hz)	125.0	132.0	132.0	130.5	131.5	131.0	130.5	131.0	131.0	131.0
		Mode#4(Hz)	867.0	877.0	959.5	1155.0	1159.0	1163.0	1163.0	1161.0	1165.0	1163.0
		Mode#5(Hz)		1233.0	1236.0							

Table 3.6 : Amplitudes in mm for different tightening torques.

			Torque value of C									
Excitation Point	**Measurement Point**	**Amplitude (m/s^2/N)**	**200 N.cm**	**600 N.cm**	**800 N.cm**	**1000 N.cm**	**1200 N.cm**	**1400 N.cm**	**1600 N.cm**	**1800 N.cm**	**2000 N.cm**	**2200 N.cm**
Tub-5	**Screw-C**	**Mode#1**	0.17	0.22	0.21	0.12	0.11	0.12	0.13	0.13	0.10	0.11
		Mode#2	1.31	1.53	1.81	1.78	1.75	1.75	1.55	1.73	1.79	1.61
		Mode#3	2.28	2.12	2.44	2.32	2.29	2.23	1.94	2.27	2.39	2.09
		Mode#4	3.40	0.22	0.19	0.49	0.46	0.62	0.69	0.68	0.66	0.73
		Mode#5		1.56	0.63							

3.3 Preload Measurement with Shaker Test

In order to determine the preload change having a certain excitation frequency, a load cell that can measure up to the load value of 20 kN is placed under the threaded fasteners. Initially, transferred preload is statically measured with a nominal tightening torque value of 2200 Ncm. Later on, a sample washing machine is placed on the base plate of an industrial vertical shaker that excites the washing machine horizontally. A brief schematic may be seen in Figure 3.16.

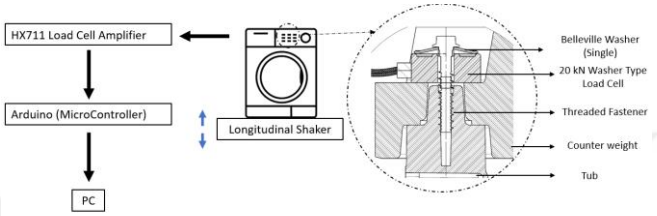

Figure 3.16 : Illustration of preload measurement with the shaker.

3.3.1 Procedure of experiment

As marked in Figure 3.3, load cells are attached to all threaded fasteners A, B and C. Preload measurement is started before tightening process in order to record the maximum preload. During the experiments, it is observed that the preload is getting lower without any shaker excitation in static loading condition. The reason for this observation is that the tub undergoes viscoelastic behavior. Therefore, before the shaking process, waiting for 10 minutes after the bolt tightening is followed to get an asymptotic value of tightening load.

3.3.2 Experimental setup

Before setting the experiment setup, the initial preload value is calculated as approximately 5 kN by using Eq. 1.1. Following, a load cell having a nominal value of 20 kN is selected, which can be seen in Figure 3.17.

Figure 3.17 : Compression load cells with 20 kN nominal value.

In initial trials, polymer tub boss crack and fracture failure were observed because of excessive stiffness increase. The reason for this is that the clamping thread length is lowered because of the thickness of the load cell. Then, in the tightening screws, the pin length of screws is increased by 20 mm.

To gather and process the data, Arduino UNO was used. With the usage of Arduino UNO, a load cell amplifier module HX711 was used in order to increase the gain of measured value in terms of voltage. An illustration of the setup for the load cell peripheral is shown in Figure 3.18.

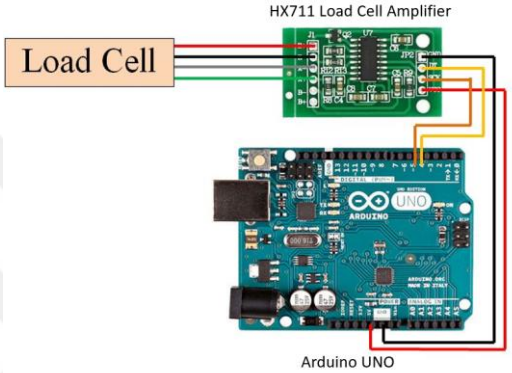

Figure 3.18 : Connection layout for the load cell, the amplifier HX711 and Arduino UNO.

The module HX711 is an amplifier which is specialized for load cell projects. The HX711 also has its own open-source library that is ready to use. After the calibration process, the load cell is mounted as shown in Figure 3.19.

Figure 3.19 : Mounted load cell.

For excitation, an industrial shaker was used which can be seen in Figure 3.20. The shaker test excitation frequency varies within 8 Hz to 100 Hz in steps. Each step's duration is 2 seconds. Detailed step table is included in Table 3.7.

Table 3.7 : Steps followed in shaker test.

Step #	Duration (seconds)	Horizontal Excitation Frequency (Hz)	Horizontal Amplitude (mm)
1	2	8	11
2	2	10	16
3	2	12	17
4	2	14	17
5	2	16	16
6	2	18	14
7	2	20	4
8	2	25	2
9	2	27	2
10	2	32	1
11	2	50	2
12	2	60	1
13	2	100	1

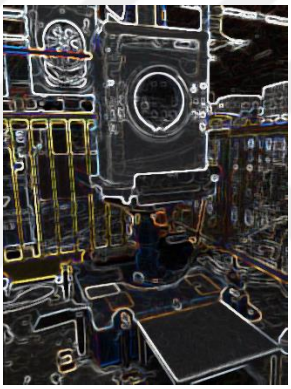

Figure 3.20 : The shaker test with a washing machine.

Shaker excitation frequency profile can be represented with a chirp function by using MATLAB. This profile can be seen in Figure 3.21.

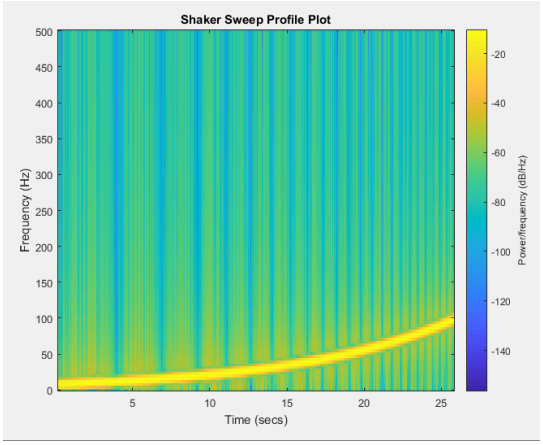

Figure 3.21 : Shaker excitation sweep profile.

3.4 Identification with Shaker Test

As expressed previously, there is a settlement time of threaded fastener preload before initiating shaker test process. When standard tightening torque value 2200 N.cm applied, maximum value of approximately 436 kg-f is recorded in static conditions Recorded values can be seen in Figure 3.23.

In torque tightening phase of screw A, THE plastic tub boss had a fracture failure, because of increased stiffness. The reason for the stiffness increase was that the clamping thread length was lowered as the load cell was mounted between flanges. Therefore, threaded screw pin length was increased as much as the thickness of the load cell, which was 20 mm. New threaded screws can be seen in Figure 3.23.

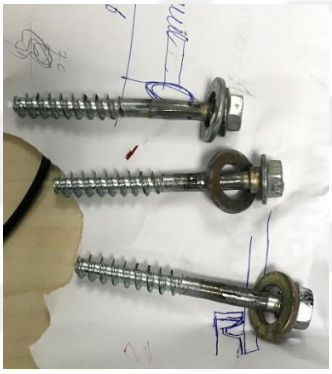

Figure 3.22 : Threaded screws with increased pin length.

After assembling the extended screws, given initial preload was increased from 4.3 kN to 7 kN. For initial measurements, steps in Table 3.7 were applied for 150 cycles. The preload measurement load cell was placed between the Screw A and the tub as shown in Figure 3.19. All of the screws were tightened with 2200 Ncm. After theb tightening process, it is seen that that torque value corresponds to the maximum preload of approximately 7 kN. After 150 cycles of shaker excitation, the preload of Screw A was decreased to 4.4 kN. The preload change over time can be seen in Figure 3.23.

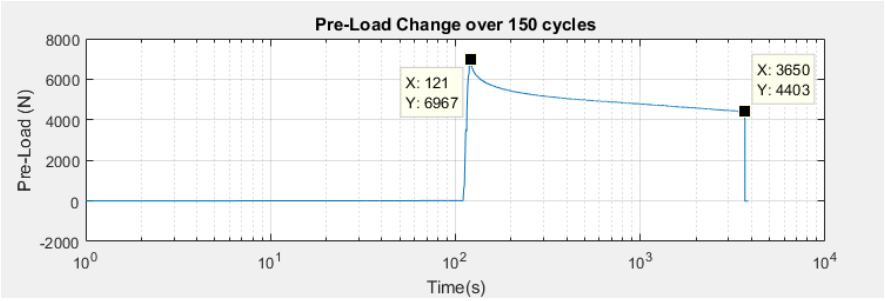

Figure 3.23 : Recorded preload decrease values during 150 cycles.

A rapid preload decrease that was about 27% of initial given preload, was observed in the first eight cycles. For further cycles, the rate of load decrease became much slower. The reason behind this behavior is interpreted as both static and dynamic effects are effective during the initial cycles. It is decided that there should be a pause before conducting the shaker experiment in order to clear out the static relaxation effect.

In further experiments, an initial pause of 1.5 hour was followed in order to observe the relaxation of preload under static load condition. After the initial pause, excitation blocks were applied. In order to examine the static effects after excitation blocks, mid-pauses also were also applied. The preload change over time can be seen in Figure 3.24.

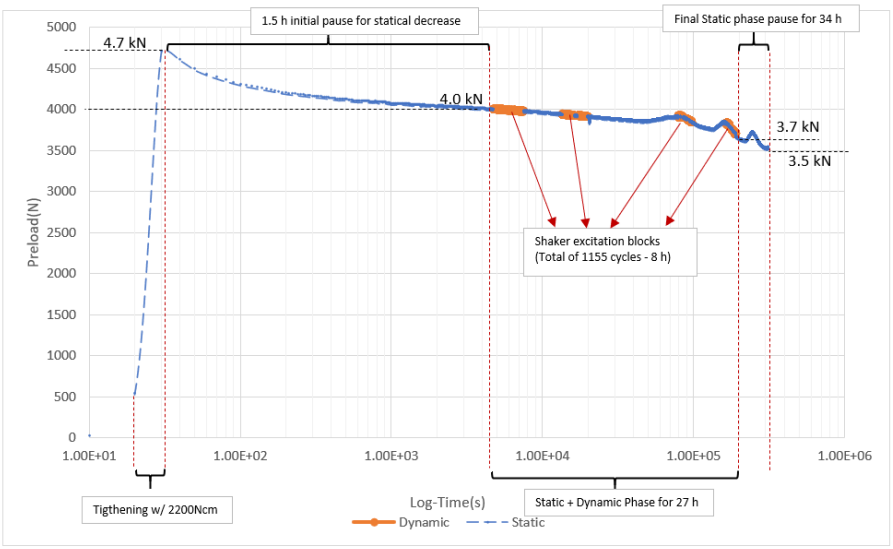

Figure 3.24 : The preload change over time.

With the tightening torque of 2200 Ncm, the screw had the initial pre-load of 4.7 kN. After the initial pause, the preload decreased to 4 kN, that was 17.5 % of initial preload. In the first excitation block, the slope of the preload decrease was similar to that of the end of the static phase. After the second excitation block, the preload had reached to a limit preload value by decreasing to 9 kN. Reaching to this limit occurred after 16 hours following the tightening process. Reaching to the extremum point is interpreted as viscoelastical characteristic of the bolt joint. In the third excitation block, the preload decreased around 0.1 kN which was 2% of the previous preload value. After the fourth excitation block, another local maximum point was observed under static loading condition. This can be explained as that the joint is affected from the previous excitations and preload history [1]. In sum, total 8 hours (1155 cycles) of excitation

was applied. The preload decreased by 25.5% with respect to the initial load. In addition, 7 local maximum and minimum points were observed. There is a relationship between the number of pauses and excitation blocks that is affecting the characteristics of joint preload decrease. Therefore, another experiment is arranged with a different set of excitation blocks.

In the second test, tightening procedures are not changed. The number of excitation blocks is increased if local extremum points are going to increase or decrease. The preload change over time in the second test can be seen in Figure 3.25.

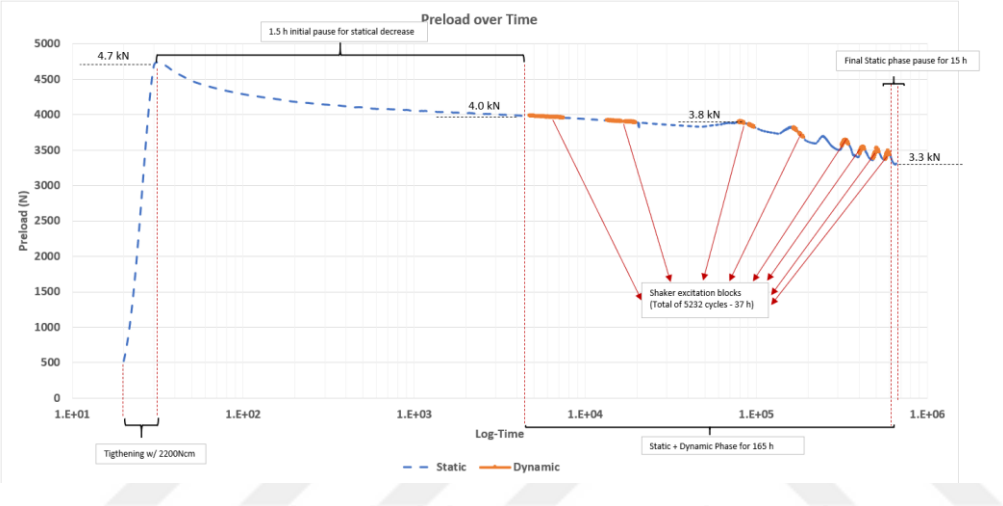

Figure 3.25 : The preload change over time in the second test.

In the second test, the preload change in static phase and the first two excitation blocks resembled to the results of the first test. Such as the previous test, viscoelastic effect is observed after the second excitation block. Before the third excitation block, the preload reached to the maximum load of 3.8 kN. As the number of excitation blocks increases, the numbers of local minimum and maximum values increase. As a resemblance from the previous test, viscoelastic behavior that can be observed in the stress history appeared after the fourth excitation block. It is also expected that this behavior is going to occur at the end of the test.

In this test, total of 105 hours (5232 cycles) shaker excitations were applied. Total preload decrease is %29.7 with respect to the initial tightening value. In viscoelastic phase, the preload decreased from 3.8 kN to 3.3 kN, that is about 13% reduction. In Figure 3.27, effect of the pause durations in the preload change with respect to excitation cycles can be seen. In this test, total of 9 excitation blocks were applied. According to that, total of 15 extremum points were observed.

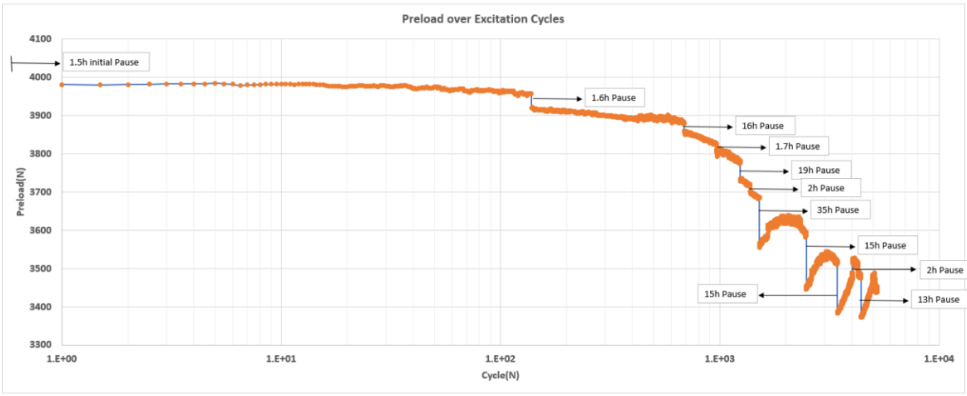

Figure 3.26 : The preload change with respect to excitation cycles.

In Figure 3.26, duration of the pause affects the joint behavior very differently. Static decrease is being very affective after 2000 cycles of excitation, especially after 35 hours of pause. This can be interpreted as stress relaxation and loosening can occur after an excitation condition. Most preload decrease (3.5 %) is observed after the cycle number of 2500, during the pause of 15 hours. As a result, the preload decrease percentage increased with an increase in the number of excitation blocks, and static pause durations are also effective on preload decrease.

4. THEORETICAL AND EXPERIMENTAL MODELING RESULT ANALYSIS

As declared previously, it is aimed that to develop a threaded fastener which can be inclined with experimental values. Firstly, from derived measurements, the RIPP method [12] will be analyzed. Secondly, with the analogy of truck leaf springs to threaded fasteners, the calculation method that is suggested by Fancher, Ervin, MacAdam, & Winkler (1980) will be used.

4.1 Analysis with the RIPP Method

In implementation of the RIPP algorithm, the approach in [12] is applied. Before implementation, parameters that are given in Table 1.2 is going to be derived with the below process in Figure 4.1 [18].

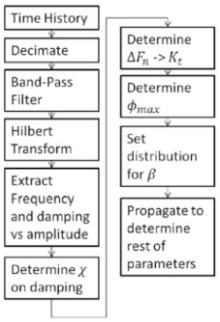

Figure 4.1 : Nonlinear parameter estimation approach [18].

Retrieved time response data of excitation point of Tub 1 and response point of Screw A is subjected above parameter extraction method around mode of 135 Hz. Initially, time response data is decimated as in Figure 4.2.

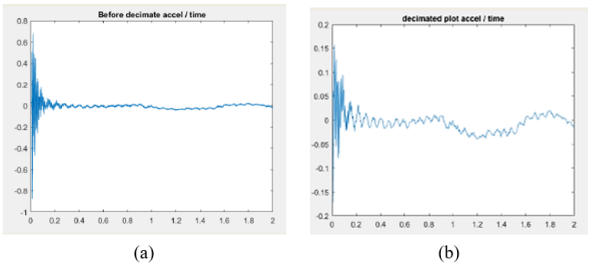

Figure 4.2 : Non-decimated data (a) and decimated data (b).

After the decimation process, time history data is band pass filtered around 135 Hz that can be seen in Figure 4.3.

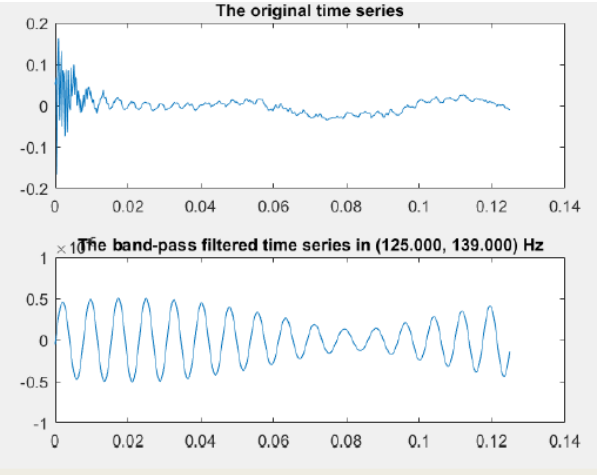

Figure 4.3 : Band pass filtered data around 135 Hz.

As mentioned in nonlinear parameter estimation algorithm, the Hilbert Transform will be applied to filtered time history data. Equation (4.1) expresses Hilbert Transform. H(u)(t) is the transformed value in domain t, where the input domain is represented by τ.

$$H(u)(t) = \frac{1}{\pi} \int_{-\infty}^{\infty} \frac{u(\tau)}{t-\tau} d\tau \tag{4.1}$$

After implementing the Hilbert transform, amplitude and phase plots are obtained as in Figure 4.4

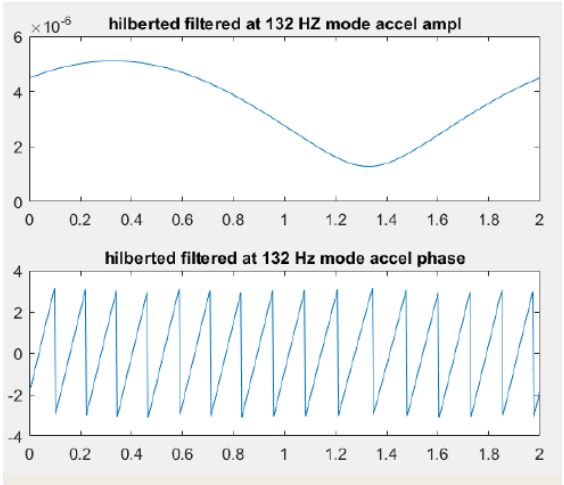

Figure 4.4 : Hilbert transformed data.

To conclude, retrieved Hilbert plots are different than the actual data in the scope of determining the non-linear parameters as mentioned in [18].

4.2 Analysis with an Analogy with Truck Leaf Springs

Fancher et al. (1980) carried out and published a study about truck leaf spring force–deflection behavior under different frequencies [17]. In sum, truck leaf springs preserve their force-deflection hysteretic curves with respect to varying frequencies in 0-15 Hz (Fig. 4.5).

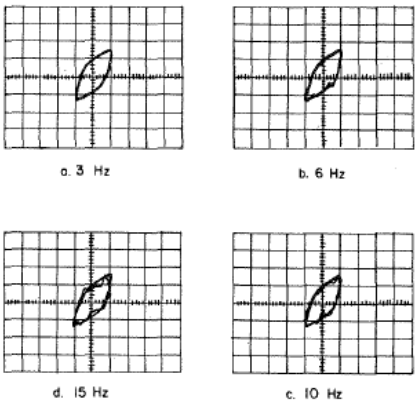

Figure 4.5 : Force deflection curves of truck leaf springs.

Reason for preservation of force–deflection characteristic can be addressed to low excitation frequencies. The same methodology can be also applied to threaded fasteners with available force–deflection hysteresis curves. Important parameters can be determined from hysteresis curve that are deflection δ, force amplitude f, hysteresis area A, equivalent stiffness K_e and average damping force C_F. The relation among these parameters can be seen in Figure 4.6 and Equations (4.2) and (4.3).

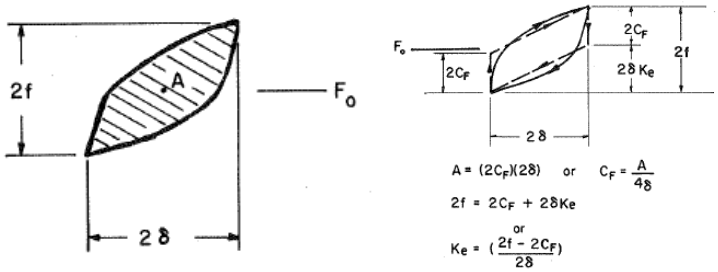

Figure 4.6 : Relations among truck spring parameters.

$$C_F = \frac{A}{4\delta} \tag{4.2}$$

$$K_e = \frac{2f - 2C_F}{2\delta} \tag{4.3}$$

In addition, Fancher et al. (1980) suggested Eq. (4.4) to describe the characteristics of truck leaf springs as follows

$$F_i = F_{ENV_i} + (F_{i-1} - F_{ENV_i})e^{-|\delta_i - \delta_{i-1}|/\beta} \tag{4.4}$$

where F_i is the reaction(suspension) force at the i^{th} time step, F_{i-1} is the reaction(suspension) force at the $i\text{-}1^{th}$ time step, δ_i is the deflection amount at the i^{th} time step, δ_{i-1} is the deflection amount at the $i\text{-}1^{th}$ time step, F_{ENVi} is the force value equivalent to upper and lower limits of the envelope at measured deflection δ_i and β is an input parameter used for describing the rate at which reaction(suspension) force within a hysteresis loop that approaches the outer limit of the envelope F_{ENV}. Using Equation (4.4), a MATLAB code is developed. With identified parameters by the code, estimated hysteresis force–deflection curve can be generated with introduced deflection– time values. In threaded fastener case, a sample force-deflection curve is produced with introduced acceleration values that are measured with an Impact Hammer Test (e.g., see Figure 4.3).

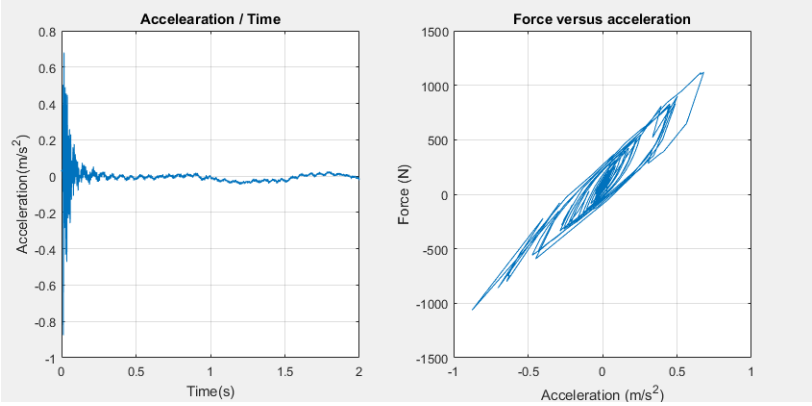

Figure 4.7 : Hysteresis curve estimation from input time response

Accordingly, estimated hysteresis curve is going to be compared with the experimental curve that is derived from preload measurement results. With the comparison of two hysteresis curves, converged parameter values will be determined.

5. CONCLUSION AND RECOMMENDATION

In this thesis, modelling of tightening and loosening mechanisms of threaded fasteners in washing machines is studied within the scope of a nonlinear frame. Particular tests and measurements are performed within the upper counter-weight part of washing machine.

5.1 General Discussion

Nonlinear dynamic behavior of threaded fasteners in washing machines is examined with Modal Testing and preload measurements. Despite other bolted joint studies, threaded connection includes a concrete body, which is used for balancing purposes, is mounted on the washing machine polymer tub. Therefore, viscoelastic effect of polymer tub is also observed. Critical modes and phase shift characteristics are determined with different pre-tightening torque values. In addition, force transmissibility of different joints is examined. Microslip and macroslip behaviors [3] are also observed which causes random phase shifts at both low and high frequencies. Joints that have low tightening torque values such as lower than 600 Ncm are experiencing distorted phase characteristics (sudden jumps in frequency domain) rather than joints that have high tightening torque values such as 1800 Ncm. Low tightening torque values are also have lower stiffness, which cause delays in force transmissibility. This condition also leads to develop an anti-resonance behavior at lower frequencies such as 32 Hz. General operating frequency of washing machines is around 27 Hz; thus, this kind of anti-resonance can increase transferred force to other connections which may cause a mechanical failure. For a washing machine, the upper counter weight connections tightened by 200 Ncm torque can be referred as critical value since the 3rd mode decreased around 7 Hz.

5.2 Further Studies

Current methods and calculations are implemented on counter-weight joints of washing machine. These methods and calculations can be used in order to develop a general model that can satisfy different connection types in washing machines. Therefore, all stiffness and damping parameters can be used as an input for finite element and computer aided engineering programs. As in the perspective of applied theoretical models, more accurate parameters are needed to be determined in order to achieve converged results. For instance, the RIPP method was originally developed and applied for lap type metal-metal joints. Since most of the washing machines have polymer material tub, viscoelastic connections is going to deliver more nonlinear characteristics to be studied.

In addition, with an extra automation algorithm, 100% joint health control method can be developed for washing machine serial productions in order to determine threaded fastener quality, with the derived modal behavior of joints in this study. Automated control approach may provide information on any threaded connection without any disassembling. By making comparisons with experimental measurements and theoretical modeling, further experimental measurements can be taken with different connection designs in order to compare critical mode frequencies and initiated preload. Processed measurements and identified parameter values can also be applied to different type of washing machines that has higher capacity and higher spin speeds.

REFERENCES

[1] **Bagley, R., & Torvik, P.** (1981). "Fractional calculus - A different approach to the finite element analysis of viscoelastically damped structures" 22nd Structures, Structural Dynamics and Materials Conference. doi: 10.2514/6.1981-484.

[2] **Bonney, M. S., Robertson, B. A., Mignolet, M., Schempp, F., & Brake, M. R.** (2016). "Experimental Determination of Frictional Interface Models" Dynamics of Coupled Structures, Volume 4 Conference Proceedings of the Society for Experimental Mechanics Series, 473–490. doi: 10.1007/978-3-319-29763-7_47

[3] **Brake, M. R. W.** (2016). "A Reduced Iwan Model that Includes Pinning for Bolted Joint Mechanics" Dynamics of Coupled Structures, Volume 4 Conference Proceedings of the Society for Experimental Mechanics Series, 231–240. doi: 10.1007/978-3-319-29763-7_22

[4] **Segalman, D. J.** (2002)**. "**A Four-Parameter Iwan Model for Lap-Type Joints" doi: 10.2172/805877

[5] **Iwan, W. D.** (1966). "A distributed-element model for hysteresis and its steady-state dynamic response" New York, NY: ASME.

[6] **Goodier, J. N., Sweeney, R. J.** (1945) **"**Loosening by Vibration of Threaded Fasteners", Mechanical Engineering, Vol. 67, 1945, pp. 798–802.

[7] **Chen, J. H., Hsieh, S. C., & Lee, A. C.** (2005). "The failure of threaded fasteners due to vibration" Proceedings of the Institution of Mechanical Engineers, Part C: Journal of Mechanical Engineering Science, 219(3), 299–314. doi: 10.1243/095440605x8450.

[8] **Junker, G. H.** (1969) "New criteria for self – loosening of fasteners under vibration" SAE International Technical Paper 690055.

[9] **The convenient and highly advantageous washing machine** (n.d.). Retrieved from http://www.deutsches-museum.de/bibliothek/unsere-schaetze/technikgeschichte/schaeffer-waschmaschine/

[10] **Bickford, J. H.** (1998) Handbook of Bolts and Bolted Joints, pp. 314-315

[11] **Fisher, J. W., Beedle, L. S.** (1966) "Bibliography on bolted and riveted structural joints" ASCE Manual No. 48 (67-15)

[12] **Brake, M. R. W.** (2018). The Mechanics of Jointed Structures Recent Research and Open Challenges for Developing Predictive Models for Structural Dynamics

[13] **Braun, S., & Ewins, D. J.** (2002). Encyclopedia of vibration

[14] **Ewins, D. J.** (2000). Modal testing: Theory and practice

[15] **Braun, S.** (2008). Discover signal processing: an interactive guide for engineers

[16] **Modal testing**(n.d.).Retrieved from<*https://www.crystalinstruments.com/modal-testing*>.

[17] **Fancher, P., Ervin, R., Macadam, C., & Winkler, C.** (1980). Measurement and Representation of the Mechanical Properties of Truck Leaf Springs. SAE Technical Paper Series. doi: 10.4271/800905

[18] **Dynamics of Coupled Structures, Volume 4**. (2016). Conference Proceedings of the Society for Experimental Mechanics Series. doi: 10.1007/978-3-319-29763-7

CURRICULUM VITAE

Name Surname **:** Onur KONUK

Place and Date of Birth **:** İzmir, 10.06.1994

E-Mail **:** onurknk94@gmail.com

EDUCATION **:**

- **B.Sc.** **:** 2017, Istanbul Technical University, Faculty of Mechanical Engineering, Mechanical Engineering Department

PROFESSIONAL EXPERIENCE AND REWARDS:

- 2017 – 2019 Arcelik A.S., Washing Machine R&D Structural Design Engineer
- 2019 – 2020 Arcelik A.S., Washing Machine Product Management Engineer
- 2020 – Present Arcelik A.S., Washing Machine R&D Structural Design Engineer